Search for Higgs bosons produced in association with *b* quarks

T. Aaltonen,[21] B. Álvarez González,[9,x] S. Amerio,[41a] D. Amidei,[32] A. Anastassov,[36] A. Annovi,[17] J. Antos,[12] G. Apollinari,[15] J. A. Appel,[15] A. Apresyan,[46] T. Arisawa,[56] A. Artikov,[13] J. Asaadi,[51] W. Ashmanskas,[15] B. Auerbach,[59] A. Aurisano,[51] F. Azfar,[40] W. Badgett,[15] A. Barbaro-Galtieri,[26] V. E. Barnes,[46] B. A. Barnett,[23] P. Barria,[44a,44c] P. Bartos,[12] M. Bauce,[41a,41b] G. Bauer,[30] F. Bedeschi,[44a] D. Beecher,[28] S. Behari,[23] G. Bellettini,[44a,44b] J. Bellinger,[58] D. Benjamin,[14] A. Beretvas,[15] A. Bhatti,[48] M. Binkley,[15,a] D. Bisello,[41a,41b] I. Bizjak,[28,bb] K. R. Bland,[5] B. Blumenfeld,[23] A. Bocci,[14] A. Bodek,[47] D. Bortoletto,[46] J. Boudreau,[45] A. Boveia,[11] L. Brigliadori,[6a,6b] A. Brisuda,[12] C. Bromberg,[33] E. Brucken,[21] M. Bucciantonio,[44a,44c] J. Budagov,[13] H. S. Budd,[47] S. Budd,[22] K. Burkett,[15] G. Busetto,[41a,41b] P. Bussey,[19] A. Buzatu,[31] C. Calancha,[29] S. Camarda,[4] M. Campanelli,[28] M. Campbell,[32] F. Canelli,[11,15] B. Carls,[22] D. Carlsmith,[58] R. Carosi,[44a] S. Carrillo,[16,l] S. Carron,[15] B. Casal,[9] M. Casarsa,[15] A. Castro,[6a,6b] P. Catastini,[20] D. Cauz,[52a] V. Cavaliere,[22] M. Cavalli-Sforza,[4] A. Cerri,[26,f] L. Cerrito,[28,r] Y. C. Chen,[1] M. Chertok,[7] G. Chiarelli,[44a] G. Chlachidze,[15] F. Chlebana,[15] K. Cho,[25] D. Chokheli,[13] J. P. Chou,[20] W. H. Chung,[58] Y. S. Chung,[47] C. I. Ciobanu,[42] M. A. Ciocci,[44a,44c] A. Clark,[18] C. Clarke,[57] G. Compostella,[41a,41b] M. E. Convery,[15] J. Conway,[7] M. Corbo,[42] M. Cordelli,[17] C. A. Cox,[7] D. J. Cox,[7] F. Crescioli,[44a,44b] C. Cuenca Almenar,[59] J. Cuevas,[9,x] R. Culbertson,[15] D. Dagenhart,[15] N. d'Ascenzo,[42,v] M. Datta,[15] P. de Barbaro,[47] S. De Cecco,[49a] G. De Lorenzo,[4] M. Dell'Orso,[44a,44b] C. Deluca,[4] L. Demortier,[48] J. Deng,[13,c] M. Deninno,[6a] F. Devoto,[21] M. d'Errico,[41a,41b] A. Di Canto,[44a,44b] B. Di Ruzza,[44a] J. R. Dittmann,[5] M. D'Onofrio,[27] S. Donati,[44a,44b] P. Dong,[15] M. Dorigo,[52a] T. Dorigo,[41a] K. Ebina,[56] A. Elagin,[51] A. Eppig,[32] R. Erbacher,[7] D. Errede,[22] S. Errede,[22] N. Ershaidat,[42,aa] R. Eusebi,[51] H. C. Fang,[26] S. Farrington,[40] M. Feindt,[24] J. P. Fernandez,[29] C. Ferrazza,[44a,44d] R. Field,[16] G. Flanagan,[46,t] R. Forrest,[7] M. J. Frank,[5] M. Franklin,[20] J. C. Freeman,[15] Y. Funakoshi,[56] I. Furic,[16] M. Gallinaro,[48] J. Galyardt,[10] J. E. Garcia,[18] A. F. Garfinkel,[46] P. Garosi,[44a,44c] H. Gerberich,[22] E. Gerchtein,[15] S. Giagu,[49a,49b] V. Giakoumopoulou,[3] P. Giannetti,[44a] K. Gibson,[45] C. M. Ginsburg,[15] N. Giokaris,[3] P. Giromini,[17] M. Giunta,[44a] G. Giurgiu,[23] V. Glagolev,[13] D. Glenzinski,[15] M. Gold,[35] D. Goldin,[51] N. Goldschmidt,[16] A. Golossanov,[15] G. Gomez,[9] G. Gomez-Ceballos,[30] M. Goncharov,[30] O. González,[29] I. Gorelov,[35] A. T. Goshaw,[14] K. Goulianos,[48] S. Grinstein,[4] C. Grosso-Pilcher,[11] R. C. Group,[55,15] J. Guimaraes da Costa,[20] Z. Gunay-Unalan,[33] C. Haber,[26] S. R. Hahn,[15] E. Halkiadakis,[50] A. Hamaguchi,[39] J. Y. Han,[47] F. Happacher,[17] K. Hara,[53] D. Hare,[50] M. Hare,[54] R. F. Harr,[57] K. Hatakeyama,[5] C. Hays,[40] M. Heck,[24] J. Heinrich,[43] M. Herndon,[58] S. Hewamanage,[5] D. Hidas,[50] A. Hocker,[15] W. Hopkins,[15,g] D. Horn,[24] S. Hou,[1] R. E. Hughes,[37] M. Hurwitz,[11] U. Husemann,[59] N. Hussain,[31] M. Hussein,[33] J. Huston,[33] G. Introzzi,[44a] M. Iori,[49a,49b] A. Ivanov,[7,p] E. James,[15] D. Jang,[10] B. Jayatilaka,[14] E. J. Jeon,[25] M. K. Jha,[6a] S. Jindariani,[15] W. Johnson,[7] M. Jones,[46] K. K. Joo,[25] S. Y. Jun,[10] T. R. Junk,[15] T. Kamon,[51] P. E. Karchin,[57] A. Kasmi,[6a] Y. Kato,[39,o] W. Ketchum,[11] J. Keung,[43] V. Khotilovich,[51] B. Kilminster,[15] D. H. Kim,[25] H. S. Kim,[25] H. W. Kim,[25] J. E. Kim,[25] M. J. Kim,[17] S. B. Kim,[25] S. H. Kim,[53] Y. K. Kim,[11] N. Kimura,[56] M. Kirby,[15] S. Klimenko,[16] K. Kondo,[56,a] D. J. Kong,[25] J. Konigsberg,[16] A. V. Kotwal,[14] M. Kreps,[24] J. Kroll,[43] D. Krop,[11] N. Krumnack,[5,m] M. Kruse,[14] V. Krutelyov,[51,d] T. Kuhr,[24] M. Kurata,[53] S. Kwang,[11] A. T. Laasanen,[46] S. Lami,[44a] S. Lammel,[15] M. Lancaster,[28] R. L. Lander,[7] K. Lannon,[37,w] A. Lath,[50] G. Latino,[44a,44b] T. LeCompte,[2] E. Lee,[51] H. S. Lee,[11] J. S. Lee,[25] S. W. Lee,[51,y] S. Leo,[44a,44b] S. Leone,[44a] J. D. Lewis,[15] A. Limosani,[14,s] C.-J. Lin,[26] J. Linacre,[40] M. Lindgren,[15] E. Lipeles,[43] A. Lister,[18] D. O. Litvintsev,[15] C. Liu,[45] Q. Liu,[46] T. Liu,[15] S. Lockwitz,[59] A. Loginov,[59] D. Lucchesi,[41a,41b] J. Lueck,[24] P. Lujan,[26] P. Lukens,[15] G. Lungu,[48] J. Lys,[26] R. Lysak,[12] R. Madrak,[15] K. Maeshima,[15] K. Makhoul,[30] S. Malik,[48] G. Manca,[27,b] A. Manousakis-Katsikakis,[3] F. Margaroli,[46] C. Marino,[24] M. Martínez,[4] R. Martínez-Ballarín,[29] P. Mastrandrea,[49a] M. E. Mattson,[57] P. Mazzanti,[6a] K. S. McFarland,[47] P. McIntyre,[51] R. McNulty,[27,j] A. Mehta,[27] P. Mehtala,[21] A. Menzione,[44a] C. Mesropian,[48] T. Miao,[15] D. Mietlicki,[32] A. Mitra,[1] H. Miyake,[53] S. Moed,[20] N. Moggi,[6a] M. N. Mondragon,[15,l] C. S. Moon,[25] R. Moore,[15] M. J. Morello,[15] J. Morlock,[24] P. Movilla Fernandez,[15] A. Mukherjee,[15] Th. Muller,[24] P. Murat,[15] M. Mussini,[6a,6b] J. Nachtman,[15,o] Y. Nagai,[53] J. Naganoma,[56] I. Nakano,[38] A. Napier,[54] J. Nett,[51] C. Neu,[55] M. S. Neubauer,[22] J. Nielsen,[26,e] L. Nodulman,[2] O. Norniella,[22] E. Nurse,[28] L. Oakes,[40] S. H. Oh,[14] Y. D. Oh,[25] I. Oksuzian,[55] T. Okusawa,[39] R. Orava,[21] L. Ortolan,[4] S. Pagan Griso,[41a,41b] C. Pagliarone,[52a] E. Palencia,[9,f] V. Papadimitriou,[15] A. A. Paramonov,[2] J. Patrick,[15] G. Pauletta,[52a,52b] M. Paulini,[10] C. Paus,[30] D. E. Pellett,[7] A. Penzo,[52a] T. J. Phillips,[14] G. Piacentino,[44a] E. Pianori,[43] J. Pilot,[37] K. Pitts,[22] C. Plager,[8] L. Pondrom,[58] K. Potamianos,[46] O. Poukhov,[13,a] F. Prokoshin,[13,z] A. Pronko,[15] F. Ptohos,[17,h] E. Pueschel,[10] G. Punzi,[44a,44b] J. Pursley,[58] A. Rahaman,[45] V. Ramakrishnan,[58] N. Ranjan,[46] I. Redondo,[29] P. Renton,[40] T. Riddick,[28] F. Rimondi,[6a,6b] L. Ristori,[44a,15] A. Robson,[19] T. Rodrigo,[9] T. Rodriguez,[43] E. Rogers,[22] S. Rolli,[54,i] R. Roser,[15] M. Rossi,[52a] F. Rubbo,[15] F. Ruffini,[44a,44c] A. Ruiz,[9] J. Russ,[10] V. Rusu,[15] A. Safonov,[51] W. K. Sakumoto,[47] Y. Sakurai,[56] L. Santi,[52a,52b] L. Sartori,[44a] K. Sato,[53] V. Saveliev,[42,v]

 © 2012 American Physical Society

A. Savoy-Navarro,[42] P. Schlabach,[15] A. Schmidt,[24] E. E. Schmidt,[15] M. P. Schmidt,[59,a] M. Schmitt,[36] T. Schwarz,[7] L. Scodellaro,[9] A. Scribano,[44a,44c] F. Scuri,[44a] A. Sedov,[46] S. Seidel,[35] Y. Seiya,[39] A. Semenov,[13] F. Sforza,[44a,44b] A. Sfyrla,[22] S. Z. Shalhout,[7] T. Shears,[27] P. F. Shepard,[45] M. Shimojima,[53,u] S. Shiraishi,[11] M. Shochet,[11] I. Shreyber,[34] A. Simonenko,[13] P. Sinervo,[31] A. Sissakian,[13,a] K. Sliwa,[54] J. R. Smith,[7] F. D. Snider,[15] A. Soha,[15] S. Somalwar,[50] V. Sorin,[4] P. Squillacioti,[44a] M. Stancari,[15] M. Stanitzki,[59] R. St. Denis,[19] B. Stelzer,[31] O. Stelzer-Chilton,[31] D. Stentz,[36] J. Strologas,[35] G. L. Strycker,[32] Y. Sudo,[53] A. Sukhanov,[16] I. Suslov,[13] K. Takemasa,[53] Y. Takeuchi,[53] J. Tang,[11] M. Tecchio,[32] P. K. Teng,[1] J. Thom,[15,g] J. Thome,[10] G. A. Thompson,[22] E. Thomson,[43] P. Ttito-Guzmán,[29] S. Tkaczyk,[15] D. Toback,[51] S. Tokar,[12] K. Tollefson,[33] T. Tomura,[53] D. Tonelli,[15] S. Torre,[17] D. Torretta,[15] P. Totaro,[41a] M. Trovato,[44a,44d] Y. Tu,[43] F. Ukegawa,[53] S. Uozumi,[25] A. Varganov,[32] F. Vázquez,[16,l] G. Velev,[15] C. Vellidis,[3] M. Vidal,[29] I. Vila,[9] R. Vilar,[9] J. Vizán,[9] M. Vogel,[35] G. Volpi,[44a,44b] P. Wagner,[43] R. L. Wagner,[15] T. Wakisaka,[39] R. Wallny,[8] S. M. Wang,[1] A. Warburton,[31] D. Waters,[28] M. Weinberger,[51] W. C. Wester III,[15] B. Whitehouse,[54] D. Whiteson,[43,c] A. B. Wicklund,[2] E. Wicklund,[15] S. Wilbur,[11] F. Wick,[24] H. H. Williams,[43] J. S. Wilson,[37] P. Wilson,[15] B. L. Winer,[37] P. Wittich,[15,h] S. Wolbers,[15] H. Wolfe,[37] T. Wright,[32] X. Wu,[18] Z. Wu,[5] K. Yamamoto,[39] J. Yamaoka,[14] T. Yang,[15] U. K. Yang,[11,q] Y. C. Yang,[25] W.-M. Yao,[26] G. P. Yeh,[15] K. Yi,[15,n] J. Yoh,[15] K. Yorita,[56] T. Yoshida,[39,k] G. B. Yu,[14] I. Yu,[25] S. S. Yu,[15] J. C. Yun,[15] A. Zanetti,[52a] Y. Zeng,[14] and S. Zucchelli[6a,6b]

(CDF Collaboration)

[1]*Institute of Physics, Academia Sinica, Taipei, Taiwan 11529, Republic of China*
[2]*Argonne National Laboratory, Argonne, Illinois 60439, USA*
[3]*University of Athens, 157 71 Athens, Greece*
[4]*Institut de Fisica d'Altes Energies, ICREA, Universitat Autonoma de Barcelona, E-08193, Bellaterra (Barcelona), Spain*
[5]*Baylor University, Waco, Texas 76798, USA*
[6a]*Istituto Nazionale di Fisica Nucleare Bologna, I-40127 Bologna, Italy*
[6b]*University of Bologna, I-40127 Bologna, Italy*
[7]*University of California, Davis, Davis, California 95616, USA*
[8]*University of California, Los Angeles, Los Angeles, California 90024, USA*
[9]*Instituto de Fisica de Cantabria, CSIC-University of Cantabria, 39005 Santander, Spain*
[10]*Carnegie Mellon University, Pittsburgh, Pennsylvania 15213, USA*
[11]*Enrico Fermi Institute, University of Chicago, Chicago, Illinois 60637, USA*
[12]*Comenius University, 842 48 Bratislava, Slovakia; Institute of Experimental Physics, 040 01 Kosice, Slovakia*
[13]*Joint Institute for Nuclear Research, RU-141980 Dubna, Russia*
[14]*Duke University, Durham, North Carolina 27708, USA*
[15]*Fermi National Accelerator Laboratory, Batavia, Illinois 60510, USA*
[16]*University of Florida, Gainesville, Florida 32611, USA*
[17]*Laboratori Nazionali di Frascati, Istituto Nazionale di Fisica Nucleare, I-00044 Frascati, Italy*
[18]*University of Geneva, CH-1211 Geneva 4, Switzerland*
[19]*Glasgow University, Glasgow G12 8QQ, United Kingdom*
[20]*Harvard University, Cambridge, Massachusetts 02138, USA*
[21]*Division of High Energy Physics, Department of Physics, University of Helsinki and Helsinki Institute of Physics, FIN-00014, Helsinki, Finland*
[22]*University of Illinois, Urbana, Illinois 61801, USA*
[23]*The Johns Hopkins University, Baltimore, Maryland 21218, USA*
[24]*Institut für Experimentelle Kernphysik, Karlsruhe Institute of Technology, D-76131 Karlsruhe, Germany*
[25]*Center for High Energy Physics: Kyungpook National University, Daegu 702-701, Korea; Seoul National University, Seoul 151-742, Korea; Sungkyunkwan University, Suwon 440-746, Korea; Korea Institute of Science and Technology Information, Daejeon 305-806, Korea; Chonnam National University, Gwangju 500-757, Korea; Chonbuk National University, Jeonju 561-756, Korea*
[26]*Ernest Orlando Lawrence Berkeley National Laboratory, Berkeley, California 94720, USA*
[27]*University of Liverpool, Liverpool L69 7ZE, United Kingdom*
[28]*University College London, London WC1E 6BT, United Kingdom*
[29]*Centro de Investigaciones Energeticas Medioambientales y Tecnologicas, E-28040 Madrid, Spain*
[30]*Massachusetts Institute of Technology, Cambridge, Massachusetts 02139, USA*
[31]*Institute of Particle Physics: McGill University, Montréal, Québec, Canada H3A 2T8; Simon Fraser University, Burnaby, British Columbia, Canada V5A 1S6; University of Toronto, Toronto, Ontario, Canada M5S 1A7; and TRIUMF, Vancouver, British Columbia, Canada V6T 2A3*
[32]*University of Michigan, Ann Arbor, Michigan 48109, USA*
[33]*Michigan State University, East Lansing, Michigan 48824, USA*

[34]*Institution for Theoretical and Experimental Physics, ITEP, Moscow 117259, Russia*
[35]*University of New Mexico, Albuquerque, New Mexico 87131, USA*
[36]*Northwestern University, Evanston, Illinois 60208, USA*
[37]*The Ohio State University, Columbus, Ohio 43210, USA*
[38]*Okayama University, Okayama 700-8530, Japan*
[39]*Osaka City University, Osaka 588, Japan*
[40]*University of Oxford, Oxford OX1 3RH, United Kingdom*
[41a]*Istituto Nazionale di Fisica Nucleare, Sezione di Padova-Trento, I-35131 Padova, Italy*
[41b]*University of Padova, I-35131 Padova, Italy*
[42]*LPNHE, Universite Pierre et Marie Curie/IN2P3-CNRS, UMR7585, Paris, F-75252 France*
[43]*University of Pennsylvania, Philadelphia, Pennsylvania 19104, USA*
[44a]*Istituto Nazionale di Fisica Nucleare Pisa, I-56127 Pisa, Italy*
[44b]*University of Pisa, I-56127 Pisa, Italy*
[44c]*University of Siena, I-56127 Pisa, Italy*
[44d]*Scuola Normale Superiore, I-56127 Pisa, Italy*
[45]*University of Pittsburgh, Pittsburgh, Pennsylvania 15260, USA*
[46]*Purdue University, West Lafayette, Indiana 47907, USA*
[47]*University of Rochester, Rochester, New York 14627, USA*
[48]*The Rockefeller University, New York, New York 10065, USA*
[49a]*Istituto Nazionale di Fisica Nucleare, Sezione di Roma 1, I-00185 Roma, Italy*
[49b]*Sapienza Università di Roma, I-00185 Roma, Italy*
[50]*Rutgers University, Piscataway, New Jersey 08855, USA*
[51]*Texas A&M University, College Station, Texas 77843, USA*
[52a]*Istituto Nazionale di Fisica Nucleare Trieste/Udine, I-34100 Trieste, I-33100 Udine, Italy*
[52b]*University of Udine, I-33100 Udine, Italy*
[53]*University of Tsukuba, Tsukuba, Ibaraki 305, Japan*
[54]*Tufts University, Medford, Massachusetts 02155, USA*
[55]*University of Virginia, Charlottesville, Virginia 22906, USA*
[56]*Waseda University, Tokyo 169, Japan*
[57]*Wayne State University, Detroit, Michigan 48201, USA*
[58]*University of Wisconsin, Madison, Wisconsin 53706, USA*

[a]Deceased.
[b]With visitor from Istituto Nazionale di Fisica Nucleare, Sezione di Cagliari, 09042 Monserrato (Cagliari), Italy.
[c]With visitor from University of California Irvine, Irvine, CA 92697, USA.
[d]With visitor from University of California Santa Barbara, Santa Barbara, CA 93106, USA.
[e]With visitor from University of California Santa Cruz, Santa Cruz, CA 95064, USA.
[f]With visitor from CERN,CH-1211 Geneva, Switzerland.
[g]With visitor from Cornell University, Ithaca, NY 14853, USA.
[h]With visitor from University of Cyprus, Nicosia CY-1678, Cyprus.
[i]With visitor from Office of Science, U.S. Department of Energy, Washington, DC 20585, USA.
[j]With visitor from University College Dublin, Dublin 4, Ireland.
[k]With visitor from University of Fukui, Fukui City, Fukui Prefecture, Japan 910-0017.
[l]With visitor from Universidad Iberoamericana, Mexico D.F., Mexico.
[m]With visitor from Iowa State University, Ames, IA 50011, USA.
[n]With visitor from University of Iowa, Iowa City, IA 52242, USA.
[o]With visitor from Kinki University, Higashi-Osaka City, Japan 577-8502.
[p]With visitor from Kansas State University, Manhattan, KS 66506, USA.
[q]With visitor from University of Manchester, Manchester M13 9PL, United Kingdom.
[r]With visitor from Queen Mary, University of London, London, E1 4NS, United Kingdom.
[s]With visitor from University of Melbourne, Victoria 3010, Australia.
[t]With visitor from Muons, Inc., Batavia, IL 60510, USA.
[u]With visitor from Nagasaki Institute of Applied Science, Nagasaki, Japan.
[v]With visitor from National Research Nuclear University, Moscow, Russia.
[w]With visitor from University of Notre Dame, Notre Dame, IN 46556, USA.
[x]With visitor from Universidad de Oviedo, E-33007 Oviedo, Spain.
[y]With visitor from Texas Tech University, Lubbock, TX 79609, USA.
[z]With visitor from Universidad Tecnica Federico Santa Maria, 110v Valparaiso, Chile.
[aa]With visitor from Yarmouk University, Irbid 211-63, Jordan.
[bb]With visitor from On leave from J. Stefan Institute, Ljubljana, Slovenia.

[59]*Yale University, New Haven, Connecticut 06520, USA*

(Received 24 June 2011; revised manuscript received 27 January 2012; published 22 February 2012)

We present a search for neutral Higgs bosons ϕ decaying into $b\bar{b}$, produced in association with b quarks in $p\bar{p}$ collisions. This process could be observable in supersymmetric models with high values of $\tan\beta$. The event sample corresponds to 2.6 fb^{-1} of integrated luminosity collected with the CDF II detector at the Fermilab Tevatron collider. We search for an enhancement in the mass of the two leading jets in events with three jets identified as coming from b quarks using a displaced vertex algorithm. A data-driven procedure is used to estimate the dijet mass spectrum of the nonresonant multijet background. The contributions of backgrounds and a possible Higgs boson signal are determined by a two-dimensional fit of the data, using the dijet mass together with an additional variable which is sensitive to the flavor composition of the three tagged jets. We set mass-dependent limits on $\sigma(p\bar{p} \to \phi b) \times \mathcal{B}(\phi \to b\bar{b})$ which are applicable for a narrow scalar particle ϕ produced in association with b quarks. We also set limits on $\tan\beta$ in supersymmetric Higgs models including the effects of the Higgs boson width.

DOI: 10.1103/PhysRevD.85.032005 PACS numbers: 14.80.Da, 12.60.Fr, 13.85.Rm

I. INTRODUCTION

The production of light Higgs bosons in association with b quarks can be significantly enhanced in the minimal supersymmetric standard model (MSSM) or extensions thereof. This occurs when $\tan\beta$, the ratio of the Higgs boson vacuum expectation values for up-type and down-type quarks, is large. For $\tan\beta \sim 40$ the cross section is expected to be a few picobarns [1], giving a production rate which could be observable in $p\bar{p}$ collisions at $\sqrt{s} = 1.96$ TeV at the Fermilab Tevatron. In large $\tan\beta$ scenarios the pseudoscalar Higgs boson A becomes degenerate with either the light (h) or heavy (H) scalar, doubling the cross section.

In the standard model (SM), the inclusive event yield of a light Higgs boson in the $b\bar{b}$ decay channel is overwhelmed by strong heavy-flavor pair production many orders of magnitude larger. For this reason, searches for $H_{\mathrm{SM}} \to b\bar{b}$ at the Tevatron rely on associated production modes like WH_{SM} and ZH_{SM} where backgrounds are restricted to those also containing a W or Z. In this paper we report on a search for $\phi \to b\bar{b}$, where ϕ represents a narrow scalar such as H_{SM} or the MSSM Higgs bosons $h/H/A$, with the associated production $b\phi$ likewise reducing the large heavy-flavor backgrounds. The production process is illustrated in Fig. 1. Results for the $b\phi$ process in the case of Higgs boson decays to $b\bar{b}$ have been previously obtained by D0 [2–4], and for inclusive or b-associated Higgs boson production in the $\tau\tau$ decay mode by CDF [5], D0 [6,7], and CMS [8].

We search for resonance decays into $b\bar{b}$ in events containing at least three b-jet candidates identified by displaced vertices (''tagged'' hereafter). As the jets resulting from the resonance decay are usually the most energetic jets in the event, we study the invariant mass of the two leading jets in E_T, denoted m_{12}. A signal would appear as an enhancement in the m_{12} spectrum. An example m_{12} distribution is shown in Fig. 2.

The background is predominantly QCD multijet production containing multiple bottom or charm quarks. Events with single pairs of heavy flavor also enter the sample when a third jet from a light quark or gluon is mistakenly tagged. We do not have precise *a priori* knowledge of the background composition and kinematics, nor do we wish to rely upon a Monte Carlo generator to reproduce it well [9–11]. We have instead developed a technique to model the m_{12} spectrum for the background in the triple-tagged sample in a data-driven manner, starting from double-tagged events.

To enhance the separation between the flavor-dependent background components and the possible resonance signal, we introduce a second quantity x_{tags}, constructed from the invariant masses of the secondary vertices constructed from the charged particle tracks in each jet, which is sensitive to the flavor composition: three bottom quark jets vs two bottom quarks and one charm quark, etc. The kinematic information in m_{12} is then complemented by flavor information in x_{tags}.

With data-driven estimates of the distributions of m_{12} and x_{tags} for the backgrounds and Monte Carlo models for the neutral scalar signal, we perform maximum-likelihood fits of the two-dimensional distribution of x_{tags} versus m_{12} in the data to test for the presence of resonances in the triple-tagged sample. These fits are used to set limits on the cross section times branching ratio for $\sigma(p\bar{p} \to b\phi) \times \mathcal{B}(\phi \to b\bar{b})$ and on $\tan\beta$ in MSSM scenarios. Although the procedure has been optimized for the case of production of a single resonance with the decay products predominantly represented by the two leading jets in the event, the results can also be interpreted in models of new physics with similar final states such as pair production of color octet scalars [12–14].

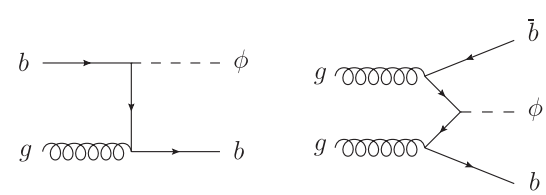

FIG. 1. Neutral scalar production in association with b quarks.

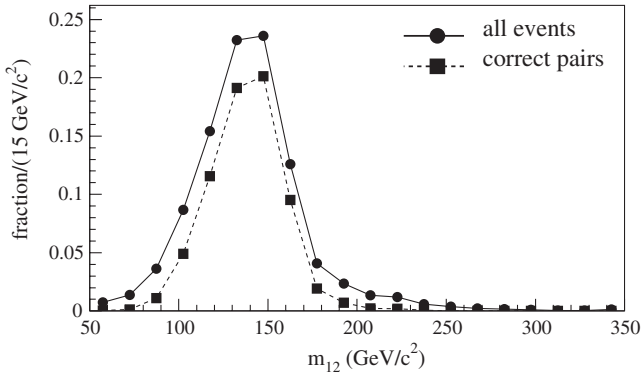

FIG. 2. The reconstructed m_{12} distribution for simulated events containing a 150 GeV/c^2 SM Higgs boson, for all events passing the selection criteria and for only those where the two leading jets represent the b quarks from the Higgs boson decay (70% of events for this mass). No backgrounds are included.

In Sec. II we briefly describe the CDF II detector subsystems upon which this analysis relies. We discuss the data sample and event selection requirements in Sec. III. A description of the signal simulation used for the search is found in Sec. IV. The data-driven background model is presented in Sec. V. The systematic uncertainties on the signal and background estimates are discussed in Sec. VI. The results for the standard model and MSSM interpretations are shown in Sec. VII. In Sec. VIII we summarize and conclude.

II. THE CDF II DETECTOR

The CDF II detector is an azimuthally and forward-backward symmetric apparatus designed to study $p\bar{p}$ collisions at the Fermilab Tevatron. Details of its design and performance are described elsewhere [15], here we briefly discuss the detector components which are relevant for this analysis. The event kinematics are described using a cylindrical coordinate system in which ϕ is the azimuthal angle, θ is the polar angle with respect to the proton beam, r is the distance from the nominal beam line, and positive z corresponds to the proton beam direction, with the origin at the center of the detector. The transverse $r - \phi$ (or $x - y$) plane is the plane perpendicular to the z axis. The pseudorapidity η is defined as $-\ln(\tan(\theta/2))$. The transverse momentum of a particle is defined as $p_T = p\sin\theta$ and the transverse energy as $E_T = E\sin\theta$.

A magnetic spectrometer consisting of tracking devices inside a 3-m diameter, 5-m long superconducting solenoidal magnet with an axial magnetic field of 1.4 T measures the momenta and trajectories of charged particles. A set of silicon microstrip detectors (L00, SVX, and ISL) [16] reconstructs charged particle trajectories in the radial range 1.5–28 cm, with a resolution on the particle position at its closest approach to the beam line of 40 μm in the transverse plane (including a 30 μm contribution from the size of the beam spot). A 3.1-m long open-cell drift chamber (COT) [17] occupies the radial range 40–137 cm. Eight superlayers of drift cells with 12 sense wires each, arranged in an alternating axial and $\pm 2°$ pattern, provide up to 96 measurements of the track position. Full radial coverage of the COT extends up to $|\eta| < 1$ and of the silicon detectors up to $|\eta| < 2$.

A sampling calorimeter system arranged in a projective-tower geometry surrounds the magnetic solenoid and covers the region up to $|\eta| < 3.6$. The calorimeter is sectioned radially into lead-scintillator electromagnetic [18] and iron-scintillator hadronic [19] compartments. The central part of the calorimeter ($|\eta| < 1.1$) is segmented in towers spanning 0.1 in η and 15° in ϕ. The forward regions ($1.1 < \eta < 3.6$) are segmented in towers spanning 0.1 to 0.64 in η, corresponding to a nearly constant 2.7° in θ. The ϕ segmentation of the forward regions is 7.5° for $1.1 < |\eta| < 2.11$ and 15° for $|\eta| > 2.11$.

Drift chambers located outside the central hadronic calorimeters and behind a 60 cm thick iron shield detect muons with $|\eta| < 0.6$ [20]. Gas Cherenkov counters with a coverage of $3.7 < |\eta| < 4.7$ measure the average number of inelastic $p\bar{p}$ collisions per beam crossing and thereby determine the luminosity [21].

III. DATA SAMPLE AND EVENT SELECTION

This analysis is based on a data sample corresponding to an integrated luminosity of 2.6 fb^{-1} collected with the CDF II detector between February 2002 and July 2008. The data are collected using a three-level trigger system. The first level requires two towers in the central calorimeter with $E_T > 5$ GeV and two tracks with $p_T > 2$ GeV/c reconstructed in the COT. The second level requires two energy clusters in the calorimeter with $E_T > 15$ GeV and $|\eta| < 1.5$ [22], along with two tracks with $p_T > 2$ GeV/c and impact parameter $|d_0| > 100$ μm, characteristic of heavy-flavor hadron decays, reconstructed using the level 2 silicon vertex trigger system [23]. The third level confirms the level 2 silicon tracks and calorimeter clusters using a variant of the offline reconstruction. No matching is required between the tracks in the silicon tracker and the calorimeter towers or clusters in the trigger system.

Because of the increasing Tevatron instantaneous luminosity profile, a higher-purity replacement for this trigger was implemented in July 2008 to stay within the constraints imposed by the CDF data acquisition system. Because the analysis is so tightly coupled to the trigger requirements, analysis of the data collected after July 2008 will require a separate dedicated study.

The offline selection requires at least three jets with $E_T > 20$ GeV and detector rapidity $|\eta| < 2$. The jets are reconstructed using a cone algorithm with radius $\Delta R = \sqrt{\Delta\phi^2 + \Delta\eta^2} < 0.7$, and are corrected for calorimeter response and multiple interactions so that the energy scale reflects the total p_T of all particles within the jet cone. In

addition, only jets containing at least two tracks within a cone of $\Delta R = 0.4$ around the jet axis satisfying the quality requirements of the displaced vertex-finding algorithm SECVTX [24] are considered. If more than three jets in the event satisfy these requirements we consider up to the fourth-leading jet in the event selection requirements (see below). Additional jets satisfying the requirements beyond the fourth-leading jet are allowed but not used in the event selection. No veto is applied for additional jets not satisfying these cuts, but they are ignored when we order the jets by E_T for the purpose of identifying the leading jets in the event. At least two of the three or four jets which are used for the event selection must match the positions of the calorimeter clusters found by the second and third levels of the trigger in η and ϕ.

The signal sample for this search is defined by requiring that the two leading jets in the event and either the third or fourth-leading jet be tagged as b-jet candidates using SECVTX. The two leading jets in the event must also match the displaced tracks required by the level 2 trigger selection. The track matching allows for the case where both tracks are matched to either of the two leading jets, or where each of the two leading jets has one of the tracks matched. The matched track requirements bias the properties of the displaced vertices found by the SECVTX algorithm. Restricting the track matching to only the two leading jets simplifies the accounting of these biases at a cost of 20–25% in efficiency relative to allowing the tracks to match any of the SECVTX-tagged jets in the event.

We also select a superset of the triple-tagged signal region by requiring both of the two leading jets, or at least one of the two leading jets and either the third or fourth-leading jet, to pass the SECVTX tag and level 2 track matching requirements. This double-tagged sample is the starting point for the background estimation procedure described in Sec. V.

We find 11 490 events passing the triple-tagged signal sample requirements. The double-tagged sample with both of the two leading jets tagged contains 267 833 events, and the sample with at least one of the two leading jets tagged and either the third or fourth jet tagged contains 424 565 events.

IV. SIGNAL MODEL

To compute the efficiency of this selection for neutral scalar signal events, the cross section of the process being searched for must be precisely defined. We use the MCFM program [25] to calculate the cross section for $bg \to H_{\rm SM} + b_{\rm jet}$ in the standard model. From this baseline the Higgs boson production rates in supersymmetric models are obtained by scaling the couplings [26,27]. If there is a gluon in the final state along with the outgoing b quark (MCFM does not simulate the Higgs boson decay) and they are within $\Delta R < 0.4$ of each other, MCFM will combine them into a "$b_{\rm jet}$"; otherwise the b quark alone serves as the jet. This $b_{\rm jet}$ is the object upon which the kinematic cuts can be applied.

We calculate the cross section for $H_{\rm SM} + b_{\rm jet}$ in the SM, requiring $p_T > 15$ GeV$/c$ and $|\eta| < 2$ for the $b_{\rm jet}$ to match the acceptance of the SECVTX algorithm. We use CTEQ6.5M [28] parton distribution functions and set the renormalization and factorization scales to $\mu_R = \mu_F = (2m_b + m_H)/4$ as suggested in Refs. [29,30]. The cross section obtained as a function of $m_{H,\rm SM}$ is shown in Fig. 3. Cross sections at the level of a femtobarn are not discernible in this final state at the Tevatron, so in the SM this process is of little interest. In the MSSM, however, simple tree-level scaling of the couplings and the degeneracy of the pseudoscalar A with one of the scalars h/H enhances this cross section by a factor of $2\tan^2\beta$. For $\tan\beta = 50$ we therefore expect cross sections of picobarns or more at the Tevatron.

The efficiency of the triple-tagged selection in events where the neutral scalar decays into a $b\bar{b}$ pair is determined from simulated data generated using the PYTHIA [31] Monte Carlo program and a full simulation of the CDF II detector [32]. We generate associated production of narrow scalars (specifically, SM Higgs bosons) with additional b quarks, and compare the kinematics of the events to the momentum and rapidity distributions predicted by the MCFM calculation. We find that the associated b jets (those not resulting from a Higgs boson decay) produced by PYTHIA are more central than is predicted by MCFM, while the other event kinematics are in good agreement. We correct the PYTHIA samples to match the MCFM predictions by reweighting the events based on the pseudorapidity of the associated b jets. Further corrections are applied in order to match the efficiencies of the SECVTX algorithm and level 2 silicon tracking requirements to those measured in the CDF data [24].

The event selection efficiencies vary from 0.3% to 1.2% as a function of the mass of the neutral scalar and are shown in Fig. 4. The efficiency of the offline requirement of three or more jets is 14–28%, the efficiency after adding the requirement of three or more SECVTX tags is

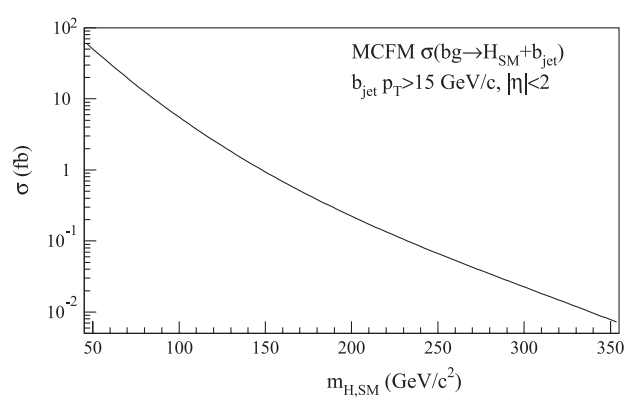

FIG. 3. Cross section for $bg \to H_{\rm SM} + b_{\rm jet}$ in the standard model calculated with MCFM.

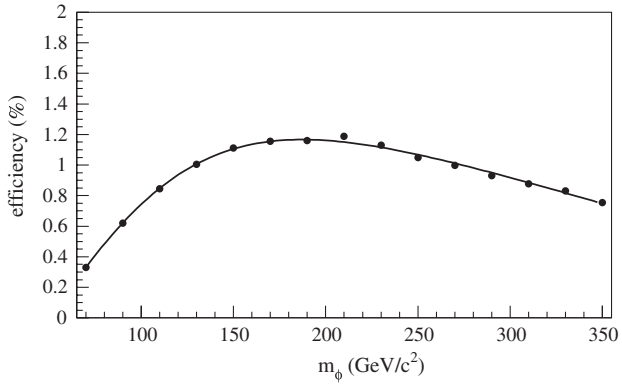

FIG. 4. Selection efficiency for $b\phi$ events as a function of the neutral scalar mass m_ϕ.

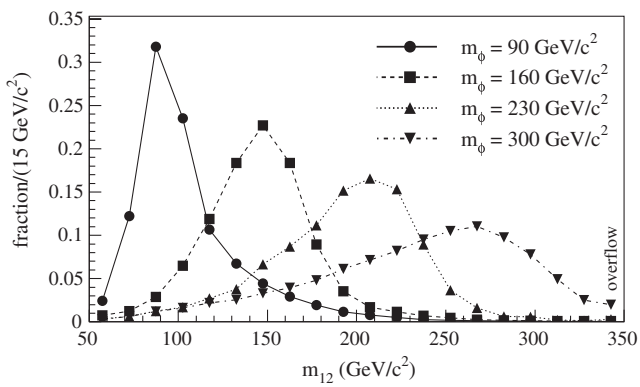

FIG. 5. Distributions of m_{12} for the simulated signal samples. The lines simply connect the bins and do not represent parametrizations. All are normalized to unit area.

0.75–1.7%, and the final matching requirements of the tagged jets to the trigger clusters and tracks reduce the efficiency to 0.3–1.2%. For a cross section of 10 pb we therefore expect to select 80–310 signal events passing our requirements. The mass of the two leading jets in the event m_{12}, which is used to separate signal from background, is shown in Fig. 5 for four values of the neutral scalar mass.

V. BACKGROUND MODEL

Aside from the possible neutral scalar signal, the triple-tagged event sample is predominantly due to the QCD multijet production of heavy quarks. Other processes such as $t\bar{t}$ production and $Z \to b\bar{b}$ + jets are found to be negligible, a point to which we shall return in Sec. VII. The heavy-flavor multijet events arise from a large number of production mechanisms [9] for which the rates are not precisely known. The differing kinematics of each can produce different m_{12} spectra, which the background estimation must accommodate. The m_{12} spectrum of the background is also affected by biases introduced by the trigger and displaced-vertex tagging requirements.

Heavy quark production can be categorized into three types of processes [9]: flavor creation, flavor excitation, and gluon splitting. Flavor creation refers to cases where a pair of heavy quarks are created directly from the hard scattering process, i.e. $q\bar{q} \to b\bar{b} + X$ where the additional activity X in the event is from initial or final state gluon radiation. Flavor excitation refers to processes with a heavy quark in the initial state which participates in the hard scattering, i.e. $bq \to bq + X$. Cases where the heavy quarks are not directly involved in the hard scattering are referred to as gluon splitting, i.e. $qg \to qg + X$ followed by $g \to b\bar{b}$ where the heavy quark pair is produced as the gluon fragments. It is possible to obtain more than two heavy quarks in the final state by combining these processes in a single event, for example $cg \to cg + X$ followed by $g \to b\bar{b}$, or $gg \to gg + X$ with both final state gluons splitting into $b\bar{b}$ pairs. Given the large number of possible final states with multiple heavy quarks, each of which can be obtained through a variety of production mechanisms, estimating the multijet background by direct calculation is a complex undertaking with potentially large uncertainties. A data-driven background estimation of the mixture of processes directly from the signal sample itself is a more tractable problem, and the method that we adopt in this analysis.

In order to qualitatively understand which of the many possible heavy quark final states are necessary to model with our data-driven method, and to what extent they differ in m_{12}, we begin with a study of simulated samples of generic QCD multijet production. These samples are generated using the PYTHIA program with MSEL = 1 ($2 \to 2$ scattering where the outgoing partons can be gluons or quarks lighter than the top quark) and a simple parametrization of the secondary vertex tagging efficiency which is a function of the E_T, pseudorapidity, and quark flavor of the jets. We find in this study that more than 90% of the QCD background in our selected triple-tag sample consists of events with at least two b jets, with the additional tagged jet being any of a mistagged light jet or a correctly tagged c jet or third b jet.

In three-jet events with at least two b jets, the additional jet is also a b jet roughly 2% of the time, a c jet 4% of the time, and a light quark or gluon jet the remaining 94% of the time. These fractions hold when the two b jets are either the two leading jets or if one of them is the third-leading jet. The flavor composition of the additional jet will ultimately be determined by fitting the data rather than using these estimates, however we will use them as starting points for the fit and also in the calculation of limits.

We next focus on the m_{12} spectrum in the subset of the PYTHIA generator-level events described above with at least two b jets. We compare the spectrum in events with two b jets and at least one other jet of any flavor to those in events where the additional jet(s) beyond the initial two b jets has a particular flavor (charm or another bottom jet). We find

no significant differences between the flavor-inclusive spectrum and the flavor-specific ones. These results hold when splitting the generated sample by heavy quark production process, so the agreement is general rather than the result of a cancellation or particular mix of processes. Changing the PYTHIA hard scattering Q^2 scale factor parameter PARP(67) over the range of 1–4 as in Ref. [9] produces significant changes in the m_{12} spectra, however the agreement between the flavor-inclusive and flavor-specific spectra is preserved as the changes in the underlying physics affect the two spectra in a similar way. In order to use PYTHIA directly to estimate the m_{12} spectrum of triple-tagged events we would need to know the "correct" values of PARP(67) and other parameters, but the similarity in m_{12} shape between double-tagged (flavor-inclusive) and triple-tagged (flavor-specific) events appears to be insensitive to the details of any particular PYTHIA tuning. All of the relevant jet physics is therefore already contained in the double-tagged sample, which can be selected from data to remove dependence on event generators such as PYTHIA. The only correction necessary to use the double-tagged events as background estimates for the triple-tagged sample is the purely instrumental bias of requiring the third tag.

Based on the results of the generator-level study, we conclude that $b\bar{b}$ plus a third-tagged jet of any flavor represents more than 90% of the heavy-flavor multijet background. This is the basis of our background model; the effect of neglecting the 10% component with fewer than two b jets is discussed in Sec. VII. Because the properties of the additional jets in $b\bar{b}$ events do not depend strongly on the flavor of the jets, we can use the sample of double-tagged events described in Sec. III as a representation for all possible flavors of the third tags.

The efficiency of requiring the third tag does depend upon the flavor, so we construct background estimates which depend on the flavor of the jet and its position in the E_T-ordered list of jets in the event. Splitting the background estimates in this way also provides flexibility to accommodate mixtures of production processes. For example, events where the two leading jets are both b jets are more likely to result from flavor creation of $b\bar{b}$ than are events with the second- and third-leading jets both b jets, which have a larger contribution from a gluon splitting to $b\bar{b}$ and recoiling against another parton from the hard scatter. The normalizations of these flavor- and topology-dependent estimates will be determined from a fit to the data so as to minimize dependence on theoretical inputs.

In the remainder of this section we show how we estimate the heavy quark multijet background from the large sample of data events with two b tags.

A. The double-tagged sample

That the triple-tagged sample predominantly contains at least two b jets is of major importance. First, it reduces the number of flavor combinations which must be considered to determine its composition to a manageable level. Secondly, samples of $b\bar{b}$ events with at least one additional jet are easily selected from the same data set as the signal region and are therefore subject to the same biases from the trigger and displaced-vertex tagging of the two b jets as the events in the signal region. By simulating the effect of the SECVTX tag on the third jet, we can use the double-tagged sample to model all components of the triple-tagged sample with two or more b jets. Because we are going to determine the normalizations from a fit to the data, we need only to model the shape of the m_{12} spectrum for each background component.

For moderate values of jet E_T SECVTX becomes more efficient as jet E_T increases, particularly for light-flavor jets where the false tag rate is highly dependent upon the number of candidate tracks in the jet which scales as the jet E_T. For b and c quark jets the effect is less dramatic, and does not hold over the full range of E_T. This effect is illustrated in Fig. 6. The drop in efficiency for b quark jets at higher E_T is due to increasing track occupancy in the jets, which causes the silicon tracker to merge hits from different tracks resulting in lower-quality tracks which are rejected by the SECVTX requirements. Because of these variations of the efficiencies as a function of jet E_T,

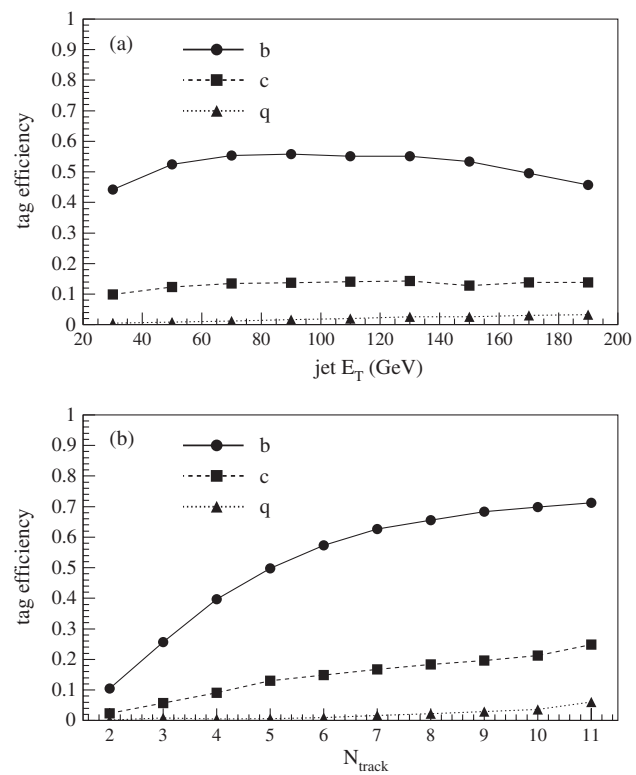

FIG. 6. Efficiency to tag a jet with the indicated flavor as a function of the jet E_T (a) and the number of tracks passing SECVTX quality requirements in the jet (b). Only jets with at least two quality tracks are included. The highest bin in each plot includes overflows.

requiring SECVTX-tagged jets will bias the events to a different m_{12} spectrum than is observed in the parent, untagged sample. The double-tagged sample which is the starting point for our background estimates already includes the bias due to the two existing tags, so we must simulate only the bias which would be due to requiring the third tag as in the signal region. This is accomplished by weighting the events using efficiency parametrizations for b, c, and light-flavor jets derived from large samples of fully-simulated PYTHIA multijet events. The efficiencies are parametrized as a function of the jet E_T and the number of tracks in the jet passing the SECVTX quality cuts. As these efficiencies are derived from simulated samples, they are corrected to match the E_T-parametrized efficiencies observed in the data using the same procedure employed for the simulated Higgs boson samples.

We describe the flavor structure of the jets in the event in the form xyz, where xy denotes the flavor of the two leading jets and z is the flavor of the third-leading jet or fourth-leading jet in the case that the third-leading jet is not tagged by SECVTX. For example, bqb would denote events where the two leading jets are a b jet (b) and a mistagged light quark (or gluon) jet (q), and the third tag is another b jet. Because our search variable m_{12} is symmetric under the interchange of the two leading jets, we make no distinction between the leading and second-leading jets so that in a bqb event the gluon or light-flavor jet q could be either of the two leading jets.

With this convention, we identify five types of event with at least two b jets. Three involve b jets in both of the leading jets: bbb, bbc, and bbq. The other two, bcb and bqb, have the non-b jet in one of the two leading jets. The distinction between the flavor content within the two leading jets and the flavor of the third jet is important, as the events will have differing kinematics and tagging biases when comparing bbq *vs.* bqb. In bbq events the two b jets are likely to have originated directly from the hard scatter, while in bqb it is more likely that the two b jets come from a gluon splitting as mentioned above. The SECVTX algorithm is much more biased toward high-E_T jets for light flavor than it is for b jets, so we expect that bqb events will have a harder m_{12} spectrum than bbq. Because we do not want to make any assumption about the rate of gluon splitting relative to $b\bar{b}$ flavor creation, we use both estimates and allow the fit of the data to determine the relative proportions.

Corrections to the double-tagged sample

While our model assumes two b jets in each event, the generator-level study described above indicates that the double-tagged events have a contribution of $\sim$10% where one or both of the tagged jets is a "mistagged" light-flavor jet. We correct for this using events which have two displaced vertices, but where one or both of the vertices are on the opposite side of the primary vertex from the jet direction. These "negative" tags are predominantly fake tags from light-flavor jets and are a product of the finite position resolution of the tracking system. We expect there to be an equal number of fake tags from this source on the default, "positive" side, together with additional contributions of fake tags from K_S/Λ and interactions with the detector material which are not present in the negative tags. The negative tags also contain a small contribution from heavy-flavor jets which should be subtracted in order to obtain the positive fake rate. The total number of positive fake tags is found by scaling the negative tag count by a factor $\lambda = 1.4 \pm 0.2$ [24] which accounts for the effects described above and is measured from the data. We find no significant variation of λ as a function of jet E_T.

We weight these events to simulate the third tag in the same way as the events with two default "positive" tags and then compute the number of true $b\bar{b}$ events using

$$N_{b\bar{b}} = N_{++} - \lambda N_{+-} + \lambda^2 N_{--} \tag{1}$$

where N_{++} is the number of observed positive double tags, N_{+-} is the number of events with one of the tags negative, and N_{--} is the number with both tags negative. This relation can be understood by considering N_{+-} as the number of events with either one b tag and one fake tag or two fake tags. The two fake tag case will be double-counted by this estimate, because there are two permutations for which jet is the positive tag and which is the negative tag. Therefore the N_{--} term which is an estimate of the number of two fake tag events is added to correct for the double-counting. The λ factors are inserted to correct the negative tag rates into estimates of the total positive fake tag rates.

This correction to subtract the non-$b\bar{b}$ component is applied bin-by-bin in m_{12} when constructing estimates

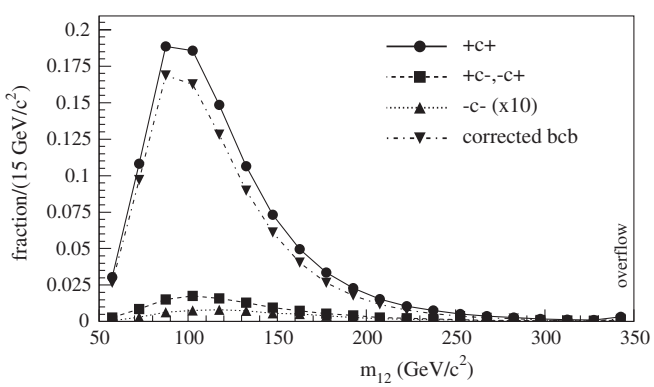

FIG. 7. Distributions of m_{12} used to construct the corrected bcb background estimate. The +c+ shape (the initial estimate with two positive tags, before correction) is shown with unit area. The +c − / − c+ shapes (starting from one positive and one negative tag) and −c− shapes (two negative tags) are shown with normalizations proportional to their area compared with +c + . For −c− a further scaling by a factor 10 is applied to enhance visibility. The corrected estimate is reduced in area by $\sim$10% relative to +c + .

for all five of the background components. It reduces the normalization by around 10% and also softens the m_{12} spectrum in each estimate, because the samples with one or two negative tags will have harder m_{12} spectra than the sample with two positive tags due to the fake tag bias towards higher jet E_T effect described above. The effect of the correction is illustrated in Fig. 7 for the bcb background estimate.

B. The heavy-flavor multijet background components

We now describe in detail how each of the five model components, or "templates", for the three-tag backgrounds is constructed from the double-tag data. When referring to the templates we adopt the convention of capitalizing the assumed flavor of the untagged jet, so that for the bbq background we would denote the template as bbQ. This distinction is most important for the bbb background as will be seen later.

1. The bbc and bbq backgrounds

Starting from the corrected double-tagged sample with the two leading jets tagged, we weight the events by the probability to tag the third jet if it were a c jet or a light-quark jet to produce estimates for the bbc and bbq background components, respectively. If a fourth jet exists, we add the weights to tag either the third or fourth jet.

2. The bcb and bqb backgrounds

The templates for these backgrounds are constructed in essentially the same way as bbC and bbQ. The difference is that we start from a double-tagged sample where one of the tags is in the third or fourth jet rather than requiring that both of the two leading jets be tagged as in bbQ/bbC. From there we subtract the non-$b\bar{b}$ component using Eq. (1) and weight the untagged jet within the two leading jets with either the charm-tag efficiency or the light-flavor jet mistag probability. The event selection requires that there be at least two level 2 trigger silicon tracks matched to the two leading jets, so, for example, in the bbQ template we require that the two leading jets contain at least two matched level 2 tracks (either at least one in each jet or at least two in one of the jets). For the bCb and bQb templates we require that only one of the two leading jets be tagged, and simulate the tag in the other jet. If the tagged jet has fewer than two matched level 2 silicon tracks, we use an efficiency parametrization for the other of the two leading jets that represents not only the efficiency to tag the jet with SECVTX (as is used in the bbQ case, for example, to simulate the fake light-flavor tag of the third or fourth jet) but also for that jet to contain enough matched level 2 silicon tracks so that the total for the two leading jets is at least two. So, for example, if the leading jet is tagged and has one matched level 2 silicon track, we would weight the event by the combined efficiency to not only tag the second-leading jet with SECVTX but also to have matched at least one level 2 silicon track to it. In this way the effect of requiring at least two matched level 2 silicon tracks within the two leading jets is modeled. In the example with one matched track in the leading jet, there must be a second level 2 silicon track somewhere in the event for it to have passed the online trigger selection. We account for this by requiring that between the two tagged jets (the leading jet and either the third- or fourth-leading in our example) there must be at least two matched level 2 silicon tracks. The requirement of the matched track in the third- or fourth-leading jet is not present in the signal sample, so this represents an unwanted bias. We remove the bias by additionally weighting these events by the ratio of the inclusive SECVTX b-jet tag efficiency for the third or fourth jet to the efficiency for SECVTX tagging with matched level 2 tracks.

3. The bbb background

The third-tag weighting procedure works straightforwardly for the bbc and bbq backgrounds, because the b-quark production physics is the same as in the bbj events used as the starting point: the b jets in the double-tagged sample can be mapped directly to the signal region and the various $b\bar{b}$ production mechanisms are properly represented. For the bbb background this is not the case, because there are two $b\bar{b}$ pairs present. Sometimes the two leading jets in the event are from the same $b\bar{b}$ pair, in which case a bbB template would be the appropriate choice because it is derived from events with the $b\bar{b}$ pair in the two leading jets. Other times the two leading jets are from a different $b\bar{b}$ pair, where a bBb template would be a better representation.

The two methods of constructing a template for bbb have significantly different m_{12} distributions, which is due to the particular kinematics of $b\bar{b}$ production through gluon splitting. Gluon splitting produces $b\bar{b}$ pairs which tend to be less back-to-back than other production mechanisms. When the two b jets in such an event are the two

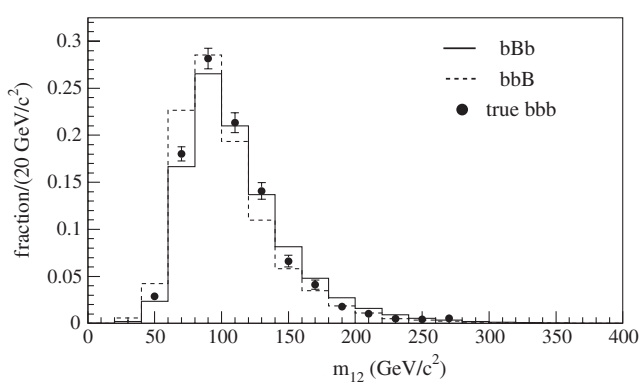

FIG. 8. Distributions of m_{12} from the generator-level PYTHIA study, for simulations of the double-tagged background templates bBb and bbB, compared to events with three true b jets.

leading jets, as in the bbB template, we observe a softer m_{12} distribution than is seen in bBb, where only one jet from the $b\bar{b}$ pair is within the two leading jets and the other of the two leading jets is an additional jet in the event against which the $b\bar{b}$ system is recoiling.

The PYTHIA simulation indicates that the m_{12} spectrum for bbb events lies between the two estimates bbB and bBb, as shown in Fig. 8. The difference between the two estimates is largest for events involving only gluon splitting, but the relationship also persists across other heavy-flavor production mechanisms. We conclude that regardless of the relative rates of $b\bar{b}$ production processes, the bbb background can be derived from an interpolation between the two templates bbB and bBb. We include both in the fit and let the data determine the proper weighting.

4. Backgrounds summary

The full set of background fit templates for m_{12} is shown in Fig. 9. Because they are too similar to discriminate in the fit, we use an average of the bbC and bbQ templates which we denote bbX. The backgrounds with two heavy-flavor jets in the leading jet pair have similar m_{12} distributions. Because the false tag rate rises with jet E_T more rapidly than does the b-tag or c-tag rate, the bQb displays a harder spectrum than bCb or bBb even though they are derived from the same events.

C. Fitting the model to the data

Our search will examine the m_{12} distribution for an enhancement riding atop the continuum background. The search will be done using a simultaneous fit for the normalization of six distributions: one neutral scalar model of varying mass, and the five background templates that together will model the background. A fit in m_{12} alone is challenged by the fact that the background templates peak at similar mass but have different widths, as seen in Fig. 9.

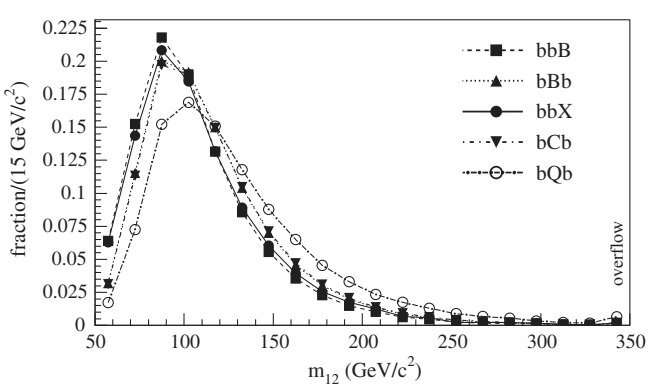

FIG. 9. Distributions of m_{12} for the background fit templates. The lines simply connect the bin centers and do not represent parametrizations. The bBb template is obscured by bCb because they have nearly the same m_{12} distribution. All are normalized to unit area.

A possible signal riding on the falling edge of the background above 100 GeV/c^2 could therefore be fitted by adding additional contribution from the wide bQb distribution, for example, resulting in loss of sensitivity. This effect can be mitigated by adding another variable which is sensitive to the differing flavor content of the templates, which we call $x_{\rm tags}$. In this section we describe the $x_{\rm tags}$ variable and then examine the ability of our background model alone to describe the data without any contribution from the neutral scalar signal model, using a two-dimensional fit of the distributions of m_{12} and $x_{\rm tags}$.

1. The flavor-dependent variable $x_{\rm tags}$

Because we are going to fit the m_{12} spectrum of the triple-tagged data with our background templates, each of which has its own characteristic m_{12} spectrum, it is useful to have a second method with which to constrain the relative fractions of each background template and obtain a firmer prediction of the overall background m_{12} spectrum. The $x_{\rm tags}$ variable should be sensitive to the flavor of the tagged jets using information independent of m_{12}.

The observable chosen as the basis of $x_{\rm tags}$ is $m_{\rm tag}$, the invariant mass of the tracks which constitute the secondary vertex as determined by SECVTX. This reflects the masses of the underlying heavy-flavor hadrons and is sensitive to the flavor of the jet as shown in Fig. 10. We define the quantity $x_{\rm tags}(m_{1,\rm tag}, m_{2,\rm tag}, m_{3,\rm tag})$, where $m_{i,\rm tag}$ is the mass of the tracks forming the displaced vertex in jet 1, 2, or 3.

For example, as mentioned above we expect that bqb events will exhibit a harder spectrum than bbq due to the bias from the fake tag in one of the two leading jets. The $x_{\rm tags}$ variable should therefore be constructed so that it is sensitive to the presence of a charm or fake tag in one of the two leading jets, using $m_{1,\rm tag}$ and $m_{2,\rm tag}$. If these events were removed, we would be left with backgrounds where the two leading jets are both b jets and the third-leading jet is any flavor. The case where the third jet is also a b jet constitutes an irreducible background to the potential neutral scalar signal in the $x_{\rm tags}$ spectrum, because the

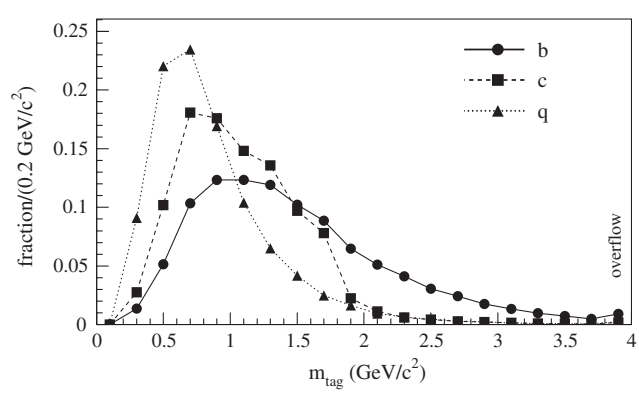

FIG. 10. The tag mass $m_{\rm tag}$ for different jet flavors, from the CDF simulation. All distributions are normalized to unit area.

signal is also three b jets. However, the backgrounds where the third jet is a charm or fake tag (bbc and bbq) can be separated from the bbb cases using $m_{3,\mathrm{tag}}$.

Because we make no distinction between the two leading jets in our flavor classification scheme, we construct x_{tags} to be symmetric under their interchange, as is m_{12}. We are interested only in the flavor combination of the pair. We choose a simple sum $m_{1,\mathrm{tag}} + m_{2,\mathrm{tag}}$ to satisfy this constraint. Combined with the information from $m_{3,\mathrm{tag}}$ we have a two-dimensional distribution, however we want to reduce this to a single variable so that when combined with m_{12} we are left with two-dimensional fit templates. To this end we define the x_{tags} variable as

$$x_{\mathrm{tags}} = \left\{ \begin{array}{ll} \min(m_{3,\mathrm{tag}}, 3): & m_{1,\mathrm{tag}} + m_{2,\mathrm{tag}} < 2 \\ \min(m_{3,\mathrm{tag}}, 3) + 3: & 2 \leq m_{1,\mathrm{tag}} + m_{2,\mathrm{tag}} < 4 \\ \min(m_{3,\mathrm{tag}}, 3) + 6: & m_{1,\mathrm{tag}} + m_{2,\mathrm{tag}} \geq 4 \end{array} \right\} \tag{2}$$

where $\min(a, b)$ returns the minimum of a and b, and all quantities are in units of GeV/c^2. The net effect is to unstack a two-dimensional histogram of $m_{1,\mathrm{tag}} + m_{2,\mathrm{tag}}$ versus $m_{3,\mathrm{tag}}$ into the one-dimensional variable x_{tags}, as illustrated in Fig. 11. The $m_{1,\mathrm{tag}} + m_{2,\mathrm{tag}}$ axis provides the sensitivity to bcb and bqb versus the other backgrounds, and the $m_{3,\mathrm{tag}}$ separates out bbc and bbq.

In order to compute x_{tags} for the background templates we need to simulate not only the efficiency of the third tag for each event, but also its expected m_{tag} spectrum. This is done by extending the tag efficiency parametrization so that it is a function of the jet E_T, the number of quality tracks, and m_{tag}. The parametrization can then be considered to represent the probability to tag a jet with a given E_T and number of quality tracks and an assumed flavor of q, c, or b, and for that tag to have a particular tag mass m_{tag}. Projections of this parametrization onto the m_{tag} axis for particular values of E_T and number of tracks are shown in Fig. 12. For each event we iterate over all bins of m_{tag} in the parametrization for the simulated third tag, compute the corresponding x_{tags} for each bin, and build up the background templates using the parametrization to estimate the appropriate weight for each value of m_{tags} in the third tag. Each event will contribute to only a single bin in m_{12} but

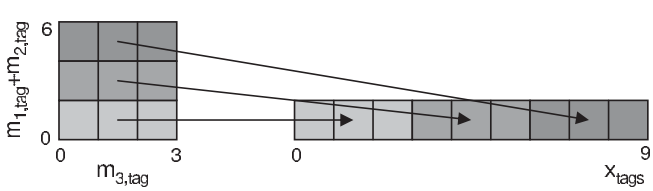

FIG. 11. Illustration of the x_{tags} definition. All axes are in units of GeV/c^2.

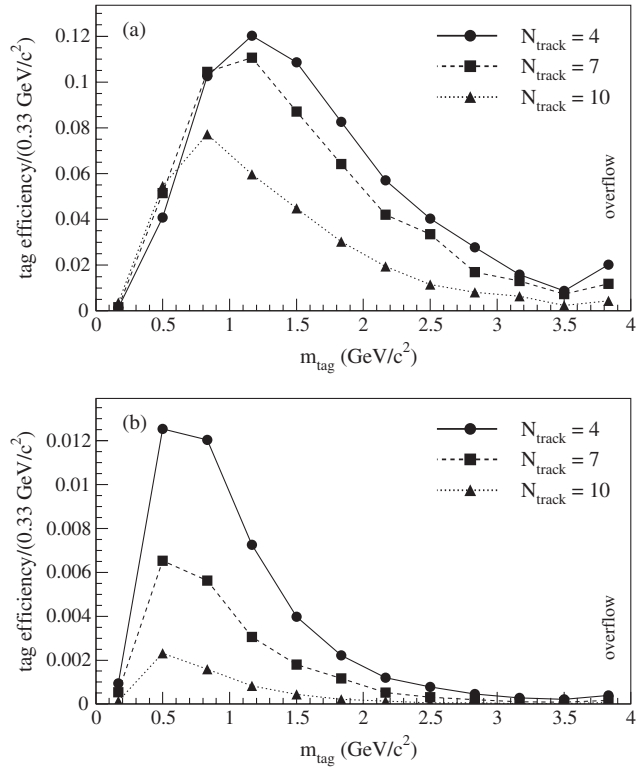

FIG. 12. Projections onto the m_{tag} axis of the tag probability parametrization, for jets with $80 < E_T < 100$ GeV and the indicated numbers of quality SECVTX tracks, for b jets (a) and fake tags of light-flavor jets (b). The area of each histogram indicates the total tag probability for this slice of E_T and number of tracks.

can fill multiple bins in x_{tags} as we iterate over the bins of m_{tag} for the third tag.

Distributions of x_{tags} for all of the background components are shown in Fig. 13. The backgrounds separate into three groups in this variable, with bCb and bQb more prominent in the bins of lower x_{tags}, bbB and bBb more prominent in the higher x_{tags} bins, and bbX with a different shape due to the non-b flavor of the tag in the third-leading jet in those events. A neutral scalar signal, because it

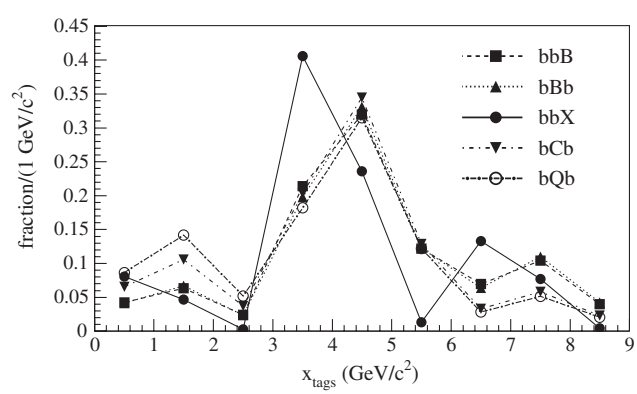

FIG. 13. Distributions of x_{tags} for the background fit templates. All are normalized to unit area.

contains three b jets, would look very similar to the bbB and bBb backgrounds in $x_{\rm tags}$.

2. Background normalization predictions

Our background model requires information only on the shapes of the various templates, with the normalizations determined from a fit to the data. However, it is possible to obtain *a priori* estimates of the normalizations, which can be used as starting points for the fit, using our templates and inputs from the generator-level PYTHIA study discussed at the beginning of this section. As constructed, the templates have total area equal to the number of $b\bar{b}$ + jet events, multiplied by the average efficiency to tag the additional jet over the entire $b\bar{b}$ + jet sample as if it were always a light-flavor, charm, or bottom jet depending on the assumed flavor. All that remains in each case is to multiply by the fraction of events where the jet truly has the assumed flavor. For the charm and bottom cases, the PYTHIA study indicates fractions of 4% and 2%, respectively.

For the light-flavor cases bbQ and bQb, we use the observed numbers of events with one or more negative tags to estimate the normalizations of these components by extending the calculation in Eq. (1) to the case of three tags

$$N_{bbQ} = N_{++-} - \lambda N_{+--} + \lambda^2 N_{---} \tag{3}$$

$$N_{bQb} = N_{+-+} - \lambda(N_{+--} + N_{--+}) + \lambda^2 N_{---} \tag{4}$$

where the N are the numbers of observed events with the indicated positive/negative tag patterns. In the case of the two leading jets containing a positive and a negative tag, for example N_{+-+}, the negative tag can be in either the first or second-leading jet. The factor λ is the same fake tag asymmetry factor used in Eq. (1).

We emphasize that these estimates are never used as constraints in any fits; the normalizations of the background components are always derived strictly from the data sample itself without any theoretical input on jet flavor fractions. We will however use these *a priori* estimates as starting points in Sec. VII for estimating the sensitivity of our search.

3. Background-only fit to the data

We fit the background and signal templates to the data using a binned maximum-likelihood fit. The likelihood function is a joint probability of the Poisson likelihood for each bin $\nu_{ij}^{n_{ij}} e^{-\nu_{ij}}/n_{ij}!$, where n_{ij} is the number of observed events in the i-th bin of m_{12} and the j-th bin of $x_{\rm tags}$, and the expectation in that bin ν_{ij} is given by

$$\nu_{ij} = \sum_b N_b f_{b,ij} + N_s f_{s,ij} \tag{5}$$

where b represents the five background templates, $f_{b,ij}$ and $f_{s,ij}$ are the bin contents of the various backgrounds (f_b) and of the neutral scalar signal (f_s), and the five N_b and optionally N_s are the free parameters of the fit which represent the normalizations of each component. We normalize all background and signal templates to unit area when performing this fit, so that the N_b and N_s parameters will correspond to the numbers of events in the sample assigned to each template.

Figure 14 shows the result of a fit of the 11 490 triple-tagged events observed in the data using only the background templates (N_s fixed to zero) and with no

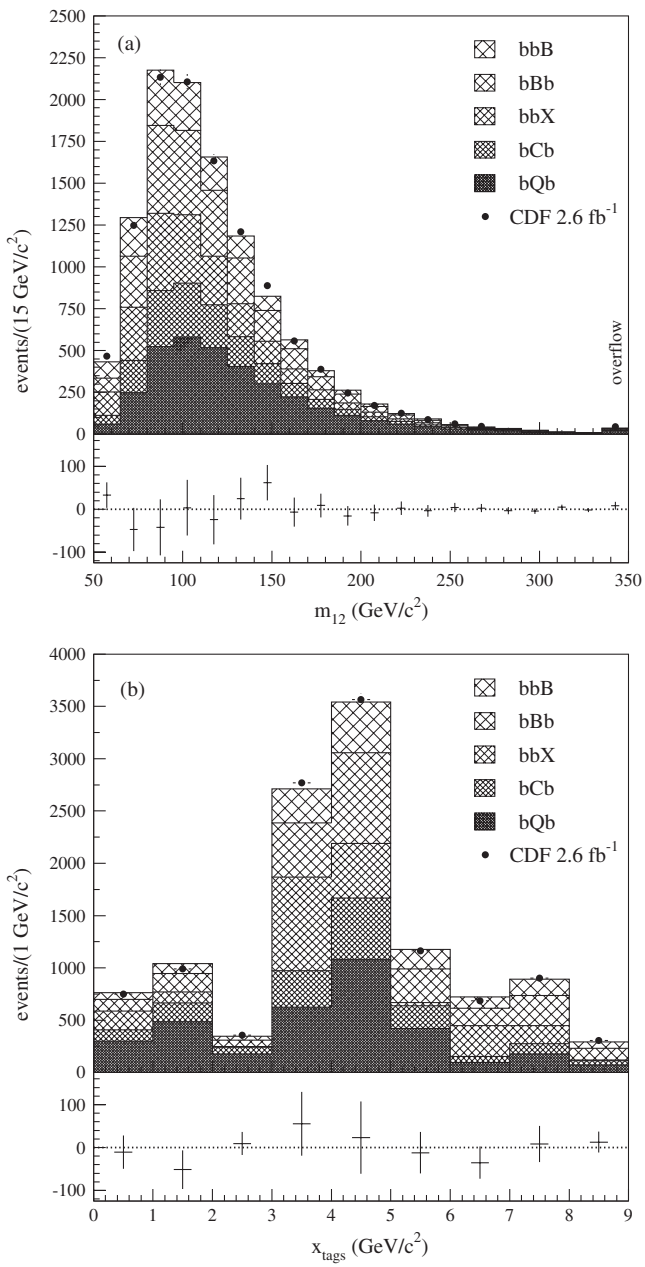

FIG. 14. Fit of the triple-tagged data sample using only the QCD background templates, in the m_{12} (a) and $x_{\rm tags}$ (b) projections. The differences between the data and the fit model are shown in the lower section of each figure.

TABLE I. Numbers of fitted events for each background type, compared to the estimates derived from the PYTHIA heavy-flavor fractions.

Component	Estimate	$N_{\rm fit}$
bbB	1300	1520 ± 540
bBb	2950	2620 ± 550
$bbX = bbQ + bbC$	$1350 + 640 = 1990$	2210 ± 160
bCb	1380	1710 ± 630
bQb	3480	3430 ± 390

systematic errors. Only the projections onto each axis are shown for clarity. The post-fit χ^2/dof between the observed data and best-fit background is $185.8/163 = 1.140$. The numbers of fitted events for each background type are given in Table I and compared to the predictions derived from the PYTHIA jet flavor fractions. Good agreement is observed for all background components. This comparison does not demonstrate the ability of PYTHIA to correctly model the m_{12} spectrum observed in the data, it tests only the overall numbers of events predicted for each flavor composition but not their kinematics. The good agreement between the fitted number of bQb events and the data-driven prediction of the normalization does indicate that we are not missing any sizeable background component with fewer than two b jets, because that component would be expected to show up at higher m_{12} values due to the bias towards high-E_T jets produced by fake tags.

In order to fully judge the quality of the background-only fit and whether it adequately describes the data, we require a framework that allows for the introduction of systematic uncertainties. We also need to be able to calculate the significance of any possible signal contribution after accounting for systematic uncertainties. The procedure we adopt uses ensembles of simulated experiments, where the simulated experiments include the effects of systematic uncertainties and the fitting procedure is the same as described above. We describe the systematic uncertainties which we consider in the next section and the simulated experiments procedure in Sec. VII.

VI. SYSTEMATIC UNCERTAINTIES

Several sources of systematic uncertainty on the signal and background contributions are considered. A summary is shown in Table II. Modeling uncertainties can affect both the normalization of the fit templates (denoted "rate" in the Table) and the distributions of m_{12} and $x_{\rm tags}$ (denoted "shape"). Shape uncertainties are introduced by modifying the templates using an interpolation procedure [33].

Rate uncertainties on the signal contribution relate to the number of signal events expected for a given cross section. They include the integrated luminosity of the data sample, the statistical errors due to the finite size of the simulated signal samples, the efficiency of the trigger and SECVTX tagging requirements, and the effect on the efficiency due to uncertainties on parton distribution functions (PDFs). For the PDF uncertainty we apply the 20 eigenvector variations of the CTEQ 6.5M set.

Modeling of the energy scale of jets introduces uncertainties both on the acceptance for signal events to pass the event selection and on the m_{12} spectrum of these events. No energy scale modeling uncertainty is assigned to the background templates since they are derived from the data.

The $x_{\rm tags}$ variable introduces an uncertainty due to modeling of the $m_{\rm tag}$ spectrum of the SECVTX displaced vertices. This uncertainty affects only the shape of the $x_{\rm tags}$ distribution and has no effect on the estimated signal acceptance. For the simulated signal events, all three SECVTX vertex masses are varied, while for the backgrounds only the mass of the simulated third tag in the event is varied because the other two tag masses in each event come directly from the data.

Varying the value of λ used to subtract the non-$b\bar{b}$ component from the double-tagged events changes the shapes of the resulting corrected background templates, and also the predicted normalizations of the bbQ and bQb templates.

We assign 50% uncertainty to the 2% (b) and 4% (c) jet flavor fractions from PYTHIA which are used to obtain the *a priori* normalization estimates of the background components. This variation is used only when throwing the simulated experiments used to estimate the sensitivity. It is

TABLE II. Summary of systematic uncertainties.

Source	Variation	Applies to	Type
Luminosity	$\pm 6\%$	Signal	Rate
Monte Carlo statistics	$\pm 2\%$	Signal	Rate
Selection efficiency	$\pm 5\%$ per jet	Signal	Rate
PDFs	$^{+3.5}_{-4.5}\,\%$	Signal	Rate
Jet energy scale	$\pm 4.5\%$	Signal	Rate/shape
b/c $m_{\rm tag}$	3%	Signal/backgrounds	Shape
Mistag $m_{\rm tag}$	3%	Backgrounds	Shape
Mistag asymmetry factor λ	1.4 ± 0.2	Backgrounds	Rate/shape
Heavy flavor fractions	$\pm 50\%$	Backgrounds	Rate

not used to constrain any of the templates in the fits. The results are largely insensitive to the size of this variation, so long as it is large relative to the precisions obtained on each template from the fit but not so large that it causes the simulated experiments to often have zero contribution from any of the background components. When performing the variation we assume that bbB and bbC are 100% correlated because they are likely to involve the same underlying physics processes; the same holds for bBb and bCb. No correlation is assumed between bbB and bBb or bbC and bCb.

VII. RESONANCE SEARCH IN THE TRIPLE-TAGGED DATA

We perform fits of the data using the background templates and templates for a neutral scalar in the mass range of 90–350 GeV$/c^2$. These fits are identical to the one shown in Fig. 14 except that in addition to floating the background normalizations we also release the constraint on the template representing a possible resonant component of the data. We use a modified frequentist CL_S method [34] to compute the sensitivity and set 95% confidence level upper limits on the cross section for production of a narrow scalar as a function of mass. We compare the data to the best-fit background plus signal model for the mass point with the most significant excess. Finally, we interpret our results as limits on $\tan\beta$ in the MSSM as a function of the pseudoscalar Higgs boson mass m_A, including the effects of the Higgs boson width.

A. Cross section times branching ratio limits

The limit calculations are performed using a custom program based on the MCLIMIT package [35]. It performs the fitting of the background and signal templates using either the observed data or simulated experiments, and calculates confidence levels using the CL_s method. The test statistic employed is the difference in χ^2 between fits using only the background templates and fits using both background and signal templates.

B. Simulated experiments

Simulated experiments are generated based on the background predictions in Table I. The number of signal events generated depends on the assumed $\sigma \times$ BR, the integrated luminosity, and the acceptance shown in Fig. 4. The predictions for the numbers of each background type and for the signal are randomly varied for each simulated experiment according to the systematic uncertainties shown in Table II. The distributions of m_{12} and $x_{\rm tags}$ are also randomly varied using histogram interpolation. The resulting background and signal templates are summed to obtain estimates for the number of events in each bin of m_{12} and $x_{\rm tags}$. These are input to a Poisson random-number generator to produce integer bin counts for the simulated experiment with the appropriate statistical variations. These are fit using the default background and signal templates to build probability densities of the test statistic for various values of $\sigma \times$ BR. The fits of either the observed data or simulated experiments always use the unmodified templates. The systematic uncertainties are only applied when building the simulated experiments.

C. Limit results

The median expected limits on $\sigma \times$ BR for statistical errors only and with full systematic uncertainties applied are shown in Table III, along with the observed limits. The systematic uncertainties increase the limits by 15–25% relative to the no-systematics case.

The expected and observed limits for the full systematics case are plotted as a function of the narrow scalar mass in Fig. 15. Also shown are the bands resulting from calculating the expected limits using the $\pm 1\sigma$ and $\pm 2\sigma$ values of the test statistic from simulated experiments containing no signal. We observe a positive deviation of greater than 2σ from the expectation in the mass region of 130–160 GeV$/c^2$. The most significant discrepancy is at

TABLE III. Median expected and observed limits on $\sigma(p\bar{p} \to b\phi) \times \mathcal{B}(\phi \to b\bar{b})$, in pb.

m_ϕ	No systematics	Full systematics	Observed
90	39.8	48.8	26.4
100	41.3	50.8	32.6
110	22.7	28.0	27.8
120	20.1	23.0	34.5
130	13.4	15.5	28.8
140	12.0	13.8	33.8
150	9.2	10.7	28.0
160	8.1	9.1	22.2
170	6.3	7.3	16.7
180	6.0	6.7	11.6
190	5.2	6.1	7.7
200	4.9	5.5	6.4
210	4.3	4.9	5.1
220	4.1	4.6	5.0
230	3.6	4.2	4.8
240	3.5	4.1	5.1
250	3.2	3.9	4.9
260	3.1	3.7	4.9
270	2.9	3.5	4.7
280	2.9	3.4	4.5
290	2.7	3.3	4.4
300	2.7	3.2	4.3
310	2.5	3.3	4.9
320	2.5	3.1	4.7
330	2.7	3.1	4.8
340	2.5	3.0	4.8
350	2.5	3.3	5.6

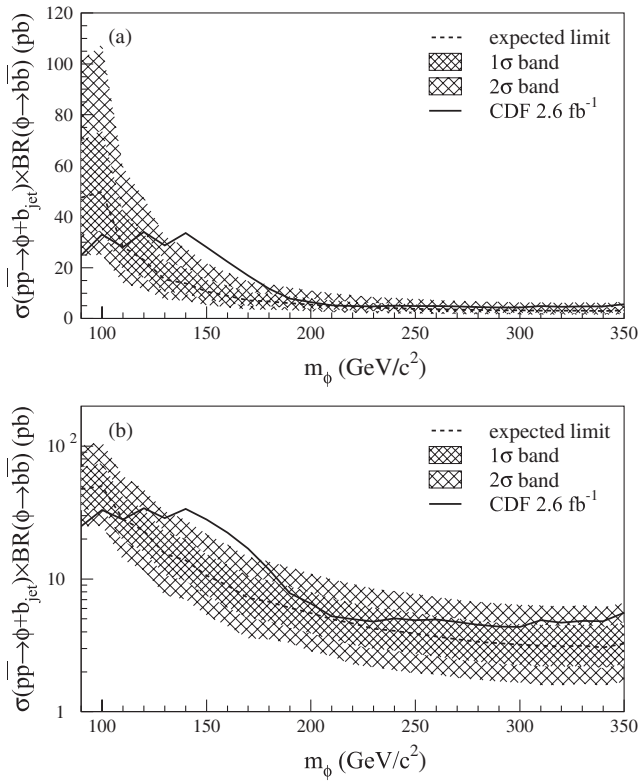

FIG. 15. Median, 1σ, and 2σ expected limits, and observed limits on narrow resonance production versus m_ϕ on linear (a) and logarithmic (b) scales.

$m_\phi = 150\ \mathrm{GeV}/c^2$, with a 1-$CL_b$ p value of 0.23%. Including the trials factor to account for the number of mass points searched, we expect to see a deviation of this magnitude at any mass in the range which we test (90–350 GeV/c^2 in steps of 10 GeV/c^2) in 2.5% of background-only pseudoexperiments.

The results of the fit of the observed data for a narrow scalar mass of 150 GeV/c^2 are shown in Fig. 16 and Table IV. In this case the χ^2/dof is $171.2/162 = 1.057$, with the fit assigning 420 ± 130 events to the signal template. If interpreted as narrow scalar production this corresponds to a cross section times branching ratio of about 15 pb within our Higgs-like production model.

TABLE IV. Numbers of fitted events for each background type and for a narrow scalar signal with $m_\phi = 150\ \mathrm{GeV}/c^2$.

Component	N_{fit}
bbB	2280 ± 600
bBb	1490 ± 670
bbX	2150 ± 160
bCb	2050 ± 630
bQb	3100 ± 400
Higgs	420 ± 130

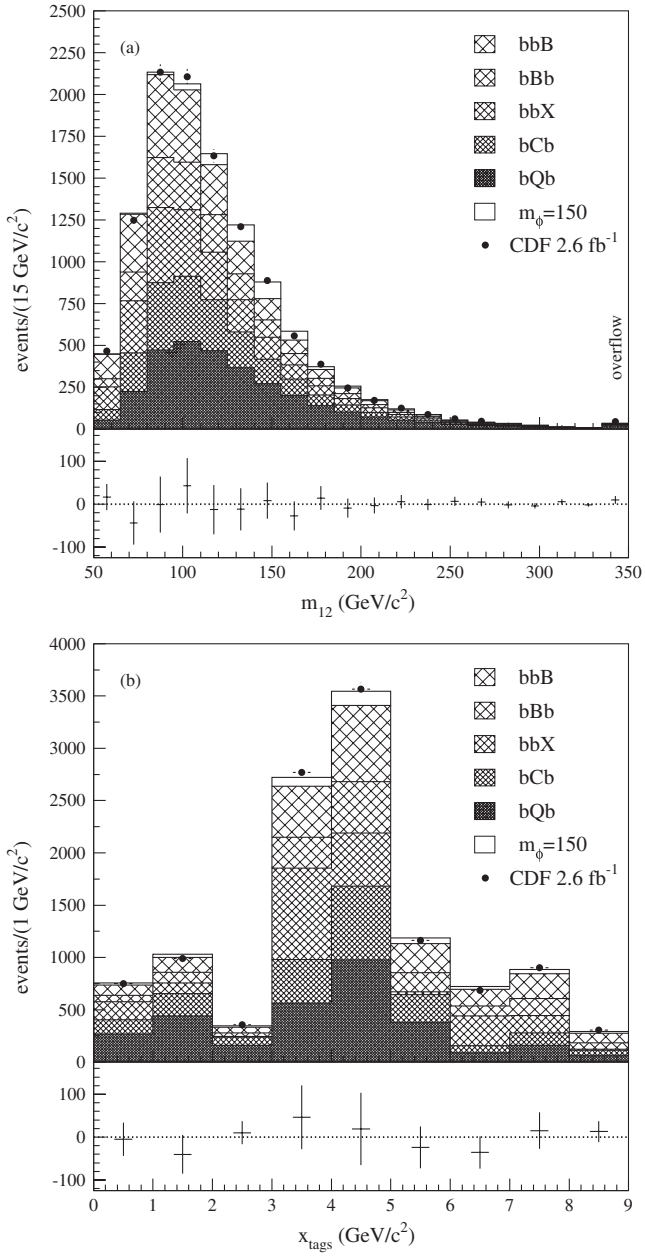

FIG. 16. Fit of the triple-tagged data sample using the QCD background templates and the signal template for $m_\phi = 150\ \mathrm{GeV}/c^2$, in the m_{12} (a) and x_{tags} (b) projections. The differences between the data and the fit model are shown in the lower section of each figure.

D. Checks of the background model

Several checks are made to investigate if the slight excess in the 140–170 GeV/c^2 mass region might be due to a neglected background contribution or mismodeling of one or more of the background templates.

One possible explanation is the effect of neglecting the component of the multijet background with fewer than two b jets. The components with at least two charm jets are found to be accommodated by residual $c\bar{c}$ contributions in

the double-tagged sample used to construct the background estimates. To check the effect of backgrounds with at least two falsely tagged light-flavor jets, we introduce a template into the fit derived from events with one positive and two negative tags. We find the fit prefers to assign $\sim 1\%$ of the sample to this template, with slightly reduced fit quality as determined from the χ^2/dof ($170.5/161 = 1.059$). The change in the fitted excess is positive and less than 5%.

We return to the question of $t\bar{t}$ pair production and $Z \to b\bar{b}$ + jets backgrounds, which are neglected in the fit. We expect around 30 and 100 events from these sources, respectively. The $Z \to b\bar{b}$ + jets background would not need to be explicitly included in the fit even if it were much larger, because it is already represented in the double-tagged events used to construct the background templates. The jets which accompany $Z \to b\bar{b}$ are similar to the jets in multijet $b\bar{b}$ + jets events, so the fraction of $Z \to b\bar{b}$ + jets in the double-tagged background sample is correctly translated into the correct fraction to account for the $Z \to b\bar{b}$ contribution to the triple-tagged signal sample. The $t\bar{t}$ contribution is also partially accounted for by this mechanism, although the jet flavor composition is not as similar due to enhanced charm production from $W \to c\bar{s}$ decays. Because of the smallness of the overall $t\bar{t}$ contribution the remaining contribution can safely be neglected.

Mismodeling of the instrumental bias introduced by simulating the effect of the third tag could distort the background templates and produce an apparent excess. We test our sensitivity to this effect by replacing the E_T-dependence of the SECVTX tag efficiency for b jets which we measured in the data with that predicted by our full detector simulation. This change is much larger than the precision with which we measure the E_T dependence in the data. Fitting the data with these modified templates, we find changes to the normalizations of the individual background templates of 50–100 events and virtually no change in the summed best-fit background model. We perform a similar test on the E_T dependence of the false tag rate used to construct the bbQ and bQb templates, in this case replacing the E_T dependence from the full detector simulation with an estimate derived from negative tags in the data. Fitting with these modified templates we find changes in the background normalizations consistent with statistical fluctuations, and again little change in the total background model.

E. MSSM interpretation

To interpret the data in MSSM scenarios, we must know the production cross section for Higgs boson events with a given pseudoscalar mass m_A as a function of $\tan\beta$. At tree level this can be computed [27] as

$$\sigma_{\mathrm{MSSM}} = 2 \times \sigma_{\mathrm{SM}} \times \tan^2\beta \times 0.9 \tag{6}$$

where σ_{SM} is the standard model cross section for a Higgs boson of mass m_A, the factor of 2 reflects the degeneracy between A and h/H, and 0.9 is the branching ratio $\mathcal{B}(A \to b\bar{b})$.

In order to go beyond tree level, we must consider the effects of loop corrections which can enhance the cross section by more or less than $\tan^2\beta$ depending upon the MSSM scenario. We must also include the effects of the Higgs boson width which can become significant when the down-type couplings are enhanced by such large factors. This means that not only the amount of signal expected but also the properties of that signal such as the reconstructed m_{12} spectrum will change depending upon the value of $\tan\beta$ in the scenario under consideration.

In Refs. [26,27] an approximate expression for the cross section times branching ratio for Higgs boson production in the MSSM, including loop effects, is given as:

$$\sigma(b\bar{b}\phi) \times \mathcal{B}(A \to b\bar{b}) \simeq 2\sigma(b\bar{b}\phi)_{\mathrm{SM}} \frac{\tan^2\beta}{(1+\Delta_b)^2} \times \frac{9}{(1+\Delta_b)^2 + 9} \tag{7}$$

where ϕ is a Higgs boson (either the SM variety or one of $h/H/A$), $\sigma(b\bar{b}\phi)_{\mathrm{SM}}$ is the SM cross section, the factor of 2 comes from the degeneracy of A with either h or H, and the loop effects are incorporated into the Δ_b parameter. For our purposes it is important only to note that Δ_b is proportional to the product of $\tan\beta$ and the Higgsino mass parameter μ. Sample values of Δ_b given in Ref. [27] are -0.21 for the $m_h^{\max}$ scenario and -0.1 for the no-mixing scenario (at $\mu = -200$ GeV and $\tan\beta = 50$). It is apparent that negative values of μ and hence of Δ_b will increase the MSSM Higgs boson yield at a given $\tan\beta$ above the tree level values and result in stronger limits on $\tan\beta$, while scenarios with μ positive will produce the opposite effect. Using Eq. (7) we can predict the Higgs boson yield for any value of $\tan\beta$ and Δ_b and therefore derive limits in any desired scenario.

The limits shown in Fig. 15 apply only to narrow scalars such as the standard model Higgs boson. If the cross section is increased by scaling the $b\bar{b}\phi$ coupling, as happens in the MSSM, then the width of the Higgs boson will increase as well. In order to account for this we convolute the cross section shown in Fig. 3 with a relativistic Breit-Wigner to produce cross section line shapes for various values of the Higgs boson pole mass, $\tan\beta$, and Δ_b. Parametrizations of the partial widths $\Gamma_{b\bar{b}}$ and $\Gamma_{\tau\tau}$ as functions of m_A and $\tan\beta$ are obtained from the FEYNHIGGS [36] program, with $\Gamma_{b\bar{b}}$ also dependent on Δ_b.

Changing the width of the Higgs boson also changes the total cross section as a function of the pole mass. We integrate the broadened cross section described above for $m_\phi > 50\ \mathrm{GeV}/c^2$ (where the acceptance for a narrow Higgs drops to zero) and divide by the cross section value expected for a narrow Higgs to derive a correction factor. This factor ranges from 1.0–0.8 for pole mass of $90\ \mathrm{GeV}/c^2$ to 1.0–1.1 for $180\ \mathrm{GeV}/c^2$, for $\tan\beta$ from

40–120. The factor drops below 1 for low pole masses because part of the broadened cross section falls below the cutoff at 50 GeV/c^2. This information is needed when computing the expected number of events for a given Higgs boson mass and $\tan\beta$ value in the limits calculator.

Fit templates for the Higgs boson signal as a function of $\tan\beta$ are constructed by combining the narrow-width templates, weighted by the line shapes and by the acceptance parametrization shown in Fig. 4. We scan over $\tan\beta$ in steps of 5 and calculate CL_s at each point, and exclude regions with $CL_s > 0.05$. The limits obtained are shown in Fig. 17 for $\Delta_b = 0$. The sensitivity begins to degrade rapidly for Higgs boson masses above 180 GeV/c^2, where the values of $\tan\beta$ required to produce an observable cross section result in an m_{12} spectrum that no longer displays a mass peak due to the large width of the Higgs boson.

Along with the $\Delta_b = 0$ case, limits are also generated for the $m_h^{\max}$ scenario with $\mu = -200$ GeV and are shown in Fig. 18. Because of the relatively large and negative values of Δ_b in this scenario, the $\tan\beta$ limits are much stronger because we expect many more signal events for a given $\tan\beta$ relative to the $\Delta_b = 0$ case. In both cases the observed limits in the mass range 120–170 GeV/c^2 are slightly above the 2σ band, due to the excess of data over the background model in this region.

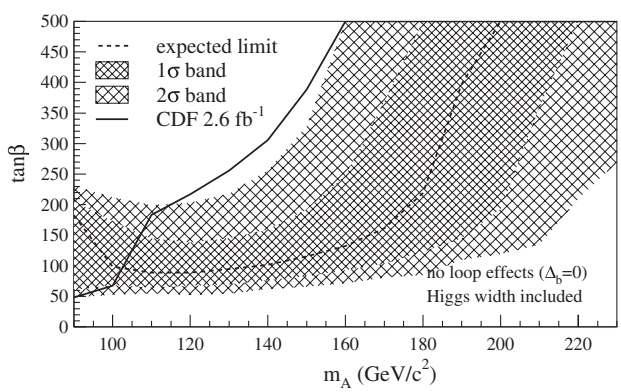

FIG. 17. Median, 1σ, and 2σ expected limits, and the observed limits versus m_A, including the Higgs boson width and for $\Delta_b = 0$.

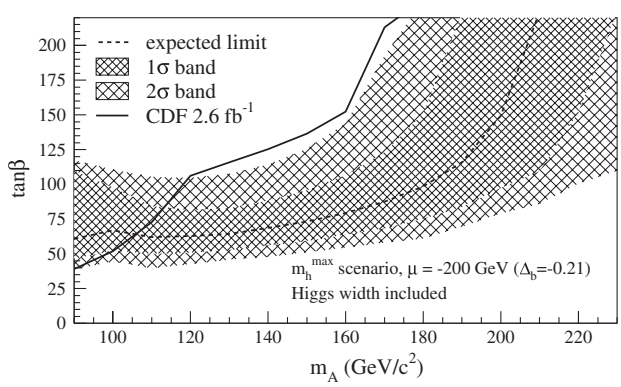

FIG. 18. Median, 1σ, and 2σ expected limits, and the observed limits versus m_A, including the Higgs boson width, for the $m_h^{\max}$ scenario with $\mu = -200$ GeV.

VIII. CONCLUSION

A search for resonances produced in association with b quarks is performed in triple-b-tagged three- or four-jet events, using 2.6 fb^{-1} of $p\bar{p}$ collisions from the Tevatron. This process could be present at a measurable rate in supersymmetric models with high values of $\tan\beta$. We use the mass of the two leading jets and jet flavor information from the secondary vertex tags to fit for a Higgs boson component within the heavy-flavor multijet background.

We find the data are consistent with the background model predictions over the entire mass range investigated. The largest deviation is observed in the mass region 140–170 GeV/c^2, where data show an excess over background with a significance of 0.23% (2.8σ) at 150 GeV/c^2. If this excess were to be attributed to the production of a narrow resonance in association with a b jet with kinematics characteristic of Higgs boson production, it would correspond to a production cross section times branching ratio of about 15 pb. We estimate the probability to observe such a deviation at any mass in the range 90–350 GeV/c^2 at 2.5% (1.9σ). Below 140 GeV/c^2 and above 170 GeV/c^2 the limits are within 2σ of expectations.

The D0 experiment published results for a similar search as the one performed here in Ref. [4]. That analysis uses a multivariate selection and discrimination procedure tuned to the MSSM Higgs boson hypothesis, whereas here a more general resonance search is performed.

The data are used to examine two MSSM scenarios. In the case where loop effects are small, we find that the growth of the Higgs boson width as the couplings are enhanced permits only weak limits of $\tan\beta > 250$ in the mass region around 150 GeV/c^2. In the $m_h^{\max}$ scenario with μ negative, the enhanced production through loop effects allows exclusion of $\tan\beta$ values greater than 40 for $m_A = 90\ \mathrm{GeV}/c^2$ and about 90–140 for the mass range 110–170 GeV/c^2. The results in Ref. [4] exclude values of $\tan\beta$ in the same $m_h^{\max}$ with μ negative scenario considered here above 50–60 over this mass range.

The MSSM study allows comparison with the results in the $A \to \tau\tau$ channel [5–8], which are much less sensitive to the details of the MSSM scenario. The $\tau\tau$ analyses exclude values of $\tan\beta$ above 25–35 in the mass range from 90–200 GeV/c^2. Any interpretation of the observed excess in the results presented here in terms of MSSM Higgs boson production would therefore be restricted to scenarios with large negative values of the Higgsino mass parameter μ, where the event yield in the $b\bar{b}$ decay mode for a given value of $\tan\beta$ is enhanced.

ACKNOWLEDGMENTS

We thank the Fermilab staff and the technical staffs of the participating institutions for their vital contributions. This work was supported by the U.S. Department of Energy and National Science Foundation; the Italian Istituto Nazionale di Fisica Nucleare; the Ministry of Education, Culture, Sports, Science and Technology of Japan; the Natural Sciences and Engineering Research Council of Canada; the National Science Council of the Republic of China; the Swiss National Science Foundation; the A. P. Sloan Foundation; the Bundesministerium für Bildung und Forschung, Germany; the Korean World Class University Program, the National Research Foundation of Korea; the Science and Technology Facilities Council and the Royal Society, UK; the Institut National de Physique Nucleaire et Physique des Particules/CNRS; the Russian Foundation for Basic Research; the Ministerio de Ciencia e Innovación, and Programa Consolider-Ingenio 2010, Spain; the Slovak R&D Agency; the Academy of Finland; and the Australian Research Council (ARC).

[1] S. Dawson, C. B. Jackson, L. Reina, and D. Wackeroth, Mod. Phys. Lett. A **21**, 89 (2006).
[2] V. M. Abazov *et al.* (D0 Collaboration), Phys. Rev. Lett. **95**, 151801 (2005).
[3] V. M. Abazov *et al.* (D0 Collaboration), Phys. Rev. Lett. **101**, 221802 (2008).
[4] V. M. Abazov *et al.* (D0 Collaboration), Phys. Lett. B **698**, 97 (2011).
[5] T. Aaltonen *et al.* (CDF Collaboration), Phys. Rev. Lett. **103**, 201801 (2009).
[6] V. M. Abazov *et al.* (D0 Collaboration), Phys. Rev. Lett. **101**, 071804 (2008).
[7] V. M. Abazov *et al.* (D0 Collaboration), Phys. Rev. Lett. **104**, 151801 (2010).
[8] S. Chatrchyan *et al.* (CMS Collaboration), Phys. Rev. Lett. **106**, 231801 (2011).
[9] D. E. Acosta *et al.* (CDF Collaboration), Phys. Rev. D **71**, 092001 (2005).
[10] T. Aaltonen *et al.* (CDF Collaboration), Phys. Rev. D **79**, 011101 (2009).
[11] D. Acosta *et al.* (CDF Collaboration), Phys. Rev. D **69**, 072004 (2004).
[12] B. A. Dobrescu, K. Kong, and R. Mahbubani, Phys. Lett. B **670**, 119 (2008).
[13] Y. Bai and B. A. Dobrescu, J. High Energy Phys. 07 (2011) 100.
[14] M. Gerbush, T. J. Khoo, D. J. Phalen, A. Pierce, and D. Tucker-Smith, Phys. Rev. D **77**, 095003 (2008).
[15] D. Acosta *et al.* (CDF Collaboration), Phys. Rev. D **71**, 032001 (2005).
[16] C. S. Hill (CDF Collaboration), Nucl. Instrum. Methods Phys. Res., Sect. A **530**, 1 (2004); A. Sill (CDF Collaboration), *ibid.* **447**, 1 (2000); A. A. Affolder *et al.* (CDF Collaboration), *ibid.* **453**, 84 (2000).
[17] A. A. Affolder *et al.* (CDF Collaboration), Nucl. Instrum. Methods Phys. Res., Sect. A **526**, 249 (2004).
[18] L. Balka *et al.* (CDF Collaboration), Nucl. Instrum. Methods Phys. Res., Sect. A **267**, 272 (1988); M. G. Albrow *et al.* (CDF Collaboration), *ibid.* **480**, 524 (2002).
[19] S. Bertolucci *et al.* (CDF Collaboration), Nucl. Instrum. Methods Phys. Res., Sect. A **267**, 301 (1988).
[20] G. Ascoli *et al.*, Nucl. Instrum. Methods Phys. Res., Sect. A **268**, 33 (1988).
[21] D. Acosta *et al.*, Nucl. Instrum. Methods Phys. Res., Sect. A **494**, 57 (2002).
[22] A. A. Bhatti *et al.*, IEEE Trans. Nucl. Sci. **56**, 1685 (2009).
[23] B. Ashmanskas *et al.* (CDF Collaboration), Nucl. Instrum. Methods Phys. Res., Sect. A **518**, 532 (2004); J. A. Adelman *et al.* (CDF Collaboration), *ibid.* **572**, 361 (2007).
[24] D. Acosta *et al.* (CDF Collaboration), Phys. Rev. D **71**, 052003 (2005).
[25] J. M. Campbell, R. K. Ellis, F. Maltoni, and S. Willenbrock, Phys. Rev. D **67**, 095002 (2003).
[26] C. Balazs, J. Diaz-Cruz, H. He, T. M. Tait, and C. Yuan, Phys. Rev. D **59**, 055016 (1999).
[27] M. Carena, S. Heinemeyer, C. E. M. Wagner, and G. Weiglein, Eur. Phys. J. C **45**, 797 (2006).
[28] W. K. Tung *et al.*, J. High Energy Phys. 02 (2007) 053.
[29] F. Maltoni, Z. Sullivan, and S. Willenbrock, Phys. Rev. D **67**, 093005 (2003).
[30] J. Campbell *et al.*, arXiv:hep-ph/0405302.
[31] T. Sjostrand *et al.*, Comput. Phys. Commun. **135**, 238 (2001); T. Sjostrand, S. Mrenna, and P. Z. Skands, J. High Energy Phys. 05 (2006) 026.
[32] E. Gerchtein and M. Paulini, in *Computing in High Energy and Nuclear Physics 2003 Conference Proceedings* eConf C0303241 (2003), p. TUMT005.
[33] A. L. Read, Nucl. Instrum. Methods Phys. Res., Sect. A **425**, 357 (1999).
[34] A. L. Read, J. Phys. G **28**, 2693 (2002).
[35] T. Junk and J. Heinrich, https://plone4.fnal.gov:4430/P0/phystat/packages/0711001.
[36] S. Heinemeyer, W. Hollik, and G. Weiglein, Comput. Phys. Commun. **124**, 76 (2000); Eur. Phys. J. C **9**, 343 (1999); G. Degrassi, S. Heinemeyer, W. Hollik, P. Slavich, and G. Weiglein, Eur. Phys. J. C **28**, 133 (2003); M. Frank *et al.*, J. High Energy Phys. 02 (2007) 047.